**MDPI**

*Review*

# Meteoric $^{10}$Be, $^{137}$Cs and $^{239+240}$Pu as Tracers of Long- and Medium-Term Soil Erosion—A Review

Aleksandra Loba [1,2,*], Jarosław Waroszewski [1], Marcin Sykuła [2], Cezary Kabala [1] and Markus Egli [3]

1   Institute of Soil Science, Plant Nutrition and Environmental Protection, Wroclaw University of Environmental and Life Sciences, Grunwaldzka 53, 50-357 Wroclaw, Poland; jaroslaw.waroszewski@upwr.edu.pl (J.W.); cezary.kabala@upwr.edu.pl (C.K.)
2   Faculty of Earth Sciences and Spatial Management, Nicolaus Copernicus University in Toruń, Lwowska 1, 87-100 Toruń, Poland; sykula@umk.pl
3   Department of Geography, University of Zurich, CH-8057 Zurich, Switzerland; markus.egli@geo.uzh.ch
*   Correspondence: aleloba@umk.pl

**Abstract:** Isotopes of meteoric $^{10}$Be, $^{137}$Cs, $^{239+240}$Pu have been proposed as a soil redistribution tracer and applied worldwide as an alternative method to classical field-related techniques (e.g., sediment traps). Meteoric $^{10}$Be provides information about long-term soil redistribution rates (millennia), while $^{137}$Cs and $^{239+240}$Pu give medium-term rates (decades). A significant progress in developing new models and approaches for the calculation of erosion rates has been made; thus, we provide a global review (n = 59) of research articles to present these three isotopes (meteoric $^{10}$Be, $^{239+240}$Pu and $^{137}$Cs) as soil erosion markers in different environments and under different land-use types. Understanding the dynamics and behaviours of isotopes in the soil environment is crucial to determine their usefulness as soil erosion tracers; thus, we discuss the chemical–physical behaviour of meteoric $^{10}$Be, $^{137}$Cs and $^{239+240}$Pu in soils. The application of these isotopes sometimes has strong limitations, and we give suggestions on how to overcome them or how to adapt them to a given situation. This review also shows where these isotopic methods can potentially be applied in the future. A lack in knowledge about soil redistribution rates exists particularly in loess-dominated areas where the tillage system has changed or in areas with strong wind erosion.

**Keywords:** isotopes; $^{239+240}$Pu; $^{137}$Cs; meteoric $^{10}$Be; RUSLE; soil erosion

## 1. Introduction

The geochemical composition of soils reflects the chemical weathering of the parent material, atmospheric deposition, dust input and biological processes [1,2]. As a result, certain elements accumulate and are preserved over time in soils in stable landforms, such as plains and low-inclination slopes [2]. However, on slopes that experience mass wasting processes, including physical mixing, erosion and downslope sediment transport, the primary distribution of elements in the soil profile is disrupted, potentially resulting in selective elemental loss or accumulation over time [2,3].

Isotopes of beryllium (meteoric $^{10}$Be), plutonium ($^{239+240}$Pu) and caesium ($^{137}$Cs) are widely used in Earth sciences to reconstruct, for example, Earth's palaeomagnetic field [4–6], snow palaeoaccumulation rates [7], seafloor sedimentation rates [8] and denudation rates [9] and to determine the age of fluvial terraces [10–12], evaluate seawater exchange cycles [13] and long-distance Asian dust transport [14], among several other processes. More recently, these isotopic tools have been used to investigate soil erosion processes in various environments, such as grasslands and forests of the European Alps or the Rocky Mountains [15–21], in arable lands, forests and grasslands of tropical and subtropical areas and the wet–dry tropics [22–26], in forested mountainous regions [21,27], forests and arable lands under continental Mediterranean climates [28–31], in moraine

landscapes used as farmlands and forests [2,32–35], in loess regions that are dominated by agriculture [36–40] or in post-fire forests and deserts areas [41,42].

The isotopes $^{10}$Be, $^{239+240}$Pu and $^{137}$Cs allow the tracing of sediment transport and erosion and deposition processes. Thus, they are essential for understanding the evolution of hillslopes and landscapes [2,43–47]. However, although they have a wide range of applications in environmental research, a comprehensive overview of meteoric $^{10}$Be, $^{239+240}$Pu and $^{137}$Cs, as soil erosion tracers, is lacking, which would facilitate identifying the most appropriate tools to study soil processes. Thus, the main aims of this review were: (1) to characterise $^{10}$Be, $^{239+240}$Pu and $^{137}$Cs as soil redistribution tracers and their chemical and physical behaviours in the soil environment; (2) to compile published worldwide articles from various environments with different types of land use where these isotopes were applied; (3) to compare erosion rates determined with isotopes with values obtained from the generally used RUSLE approach and (4) to show potential future applications.

## 2. Chemical Mechanisms and Behaviour Isotopes of $^{10}$Be, $^{239+240}$Pu and $^{137}$Cs

Understanding the dynamics and behaviours of isotopes in the soil environment is crucial to determining their usefulness as soil erosion tracers [48,49]. Therefore, in this section, we present the origin of meteoric $^{10}$Be, $^{137}$Cs and $^{239+240}$Pu and their chemistry and distribution in soils.

### 2.1. Formation of Meteoric $^{10}$Be

Meteoric $^{10}$Be is a cosmogenic radionuclide, produced constantly in the upper atmosphere and at the Earth's surface as a result of the spallation of $^{14}$N and $^{16}$O by high-energy cosmic rays to form $^{10}$BeO or $^{10}$Be(OH)$_2$ [50–52] (Figure 1 and Table 1). $^{10}$Be formed in the atmosphere is adsorbed onto aerosols and is primarily delivered to the Earth's surface by wet and dry deposition [48,52,53]. The fluxes of $^{10}$Be mainly depend on the precipitation rates and/or latitude [54,55]. At high latitudes, the precipitation rates are very low, which limit the meteoric $^{10}$Be flux, whereas, at mid-latitudes, the precipitation tends to be higher; thus, $^{10}$Be deposition is also higher [53,54]. Dry deposition is less important, because it represents <10% of the total $^{10}$Be flux, except in areas with very low precipitation rates, such as deserts or the inner part of Antarctica [52–54,56].
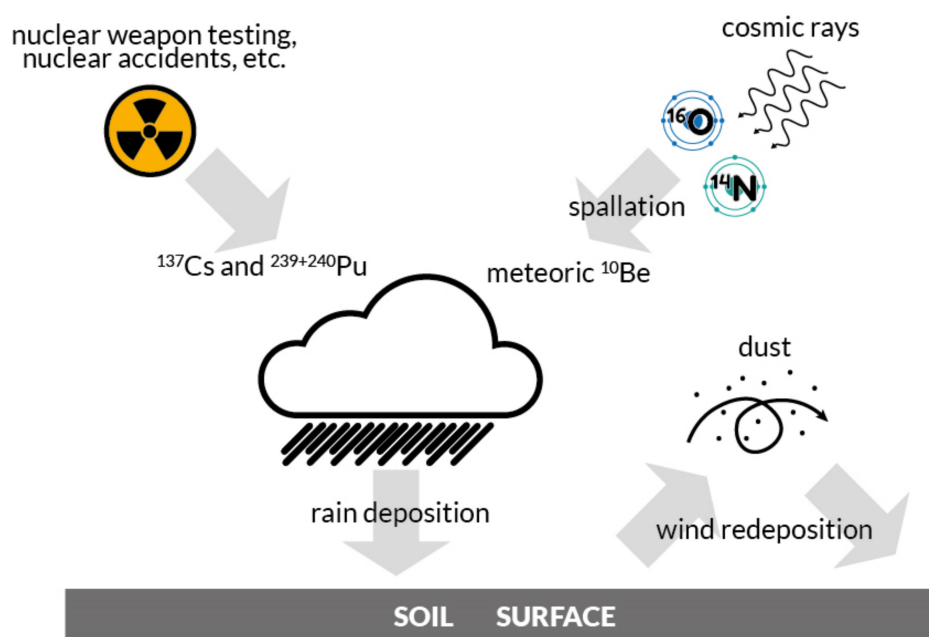


**Figure 1.** Origin of meteoric $^{10}$Be, $^{137}$Cs and $^{239+240}$Pu in soils.

**Table 1.** Comparison of $^{10}$Be, $^{137}$Cs and $^{239+240}$Pu characteristics.

| | Meteoric $^{10}$Be | $^{239+240}$Pu | $^{137}$Cs |
|---|---|---|---|
| Element category | alkaline earth metal | actinide metal | alkali metal |
| Oxidation state | II | III, IV, V and VI | I |
| Origin | cosmogenic radionuclide that is constantly produced by the spallation of oxygen and nitrogen by cosmic rays in the upper atmosphere and at the Earth's surface | distributed globally due to nuclear weapon fabrication and testing and nuclear power plants accidents, as well as nuclear fuel reprocessing | distributed globally due to nuclear weapon fabrication and testing, nuclear power plants accidents, as well as nuclear fuel reprocessing |
| Adsorption | on clay and fine particles, organic matter | associated with organic matter, sesquioxides and clay particles | mostly bound to the fine mineral (clay) fraction |
| Half-life | 1.387 Myr | $^{239}$Pu 24 110 y and $^{240}$Pu 6561 y | 30.17 y |
| Time range in erosion studies | long-term erosion rates (millennia) | medium-term erosion rates (50–60 years) | medium-term erosion rates (50–60 years) |
| Measurement | AMS | ICP-MS and AMS | gamma-ray spectrometry (counting the 662 keV gamma line), ICP MS |
| Remarks | The depth distribution of meteoric $^{10}$Be might be used to assess the occurrence of soil-mixing processes. | New tool which has been applied since more than one decade in a few countries. Proposed as an alternative to $^{137}$Cs. | Difficulties in application in large part of Europe due to heterogeneous fallout caused by the Chernobyl accident. Moreover, due to short half-life over 70% of $^{137}$Cs decayed. |
| | | The depth distribution might be used to assess the occurrence of soil-mixing processes. | The depth distribution might be used to assess the occurrence of soil-mixing processes. |

## 2.2. Meteoric $^{10}$Be in Soils

After deposition, meteoric $^{10}$Be is steadily adsorbed on clay and fine-particle surfaces having a diameter 0–2 μm (Figures 2 and 3) [37,52,57,58]. The Spearman's rank correlation coefficient based on data from various environments ($n$ = 59) also confirms the strong correlation between $^{10}$Be and the clay fraction (Figure 3). The magnitude of the adsorbed amount of beryllium is ultimately driven by the sorption capacity system [58]. The adsorption potential and, thus, the fixation of meteoric $^{10}$Be in soils depends on pH, soil texture, organic matter, the oxyhydroxide content and its cation exchange capacity [2,48,59,60]. An increase in pH caused a net increase in the negative surface charge and related enhanced affinity for metal ions; thus, the cation exchange capacity also increased [61]. At a soil pH over 4, and in the absence of organic acids, $^{10}$Be mostly occurs as hydrolysed species: BeOH$^+$, Be(OH)$_2$ and Be(OH)$_3$$^-$ (Figure 4) that are reactive and, thus, are readily adsorbed onto clay minerals.

Accumulation of meteoric $^{10}$Be begins in the upper part of soil (because it reaches the surface with rainwater), from where it penetrates to greater depths until the whole soil column is saturated [53]. Willenbring and von Blackenburg [52], however, stated that concentrations of $^9$Be and $^{10}$Be in soils are too low to saturate the adsorption site; thus, a rather partial release of $^{10}$Be occurs when pH < 4 and Be$^{2+}$ competes with dissolved Al$^{3+}$ for the exchange sites. In such acidic soils, $^{10}$Be may be translocated to a greater soil or saprolite depth or lost through leaching [25]. Nevertheless, meteoric $^{10}$Be still can be used for soil denudation research in acidic environments when its loss can be estimated [25,62]. Although some of the factors that influence the behaviour of meteoric $^{10}$Be are described above, some of the mechanisms still need a better explanation.
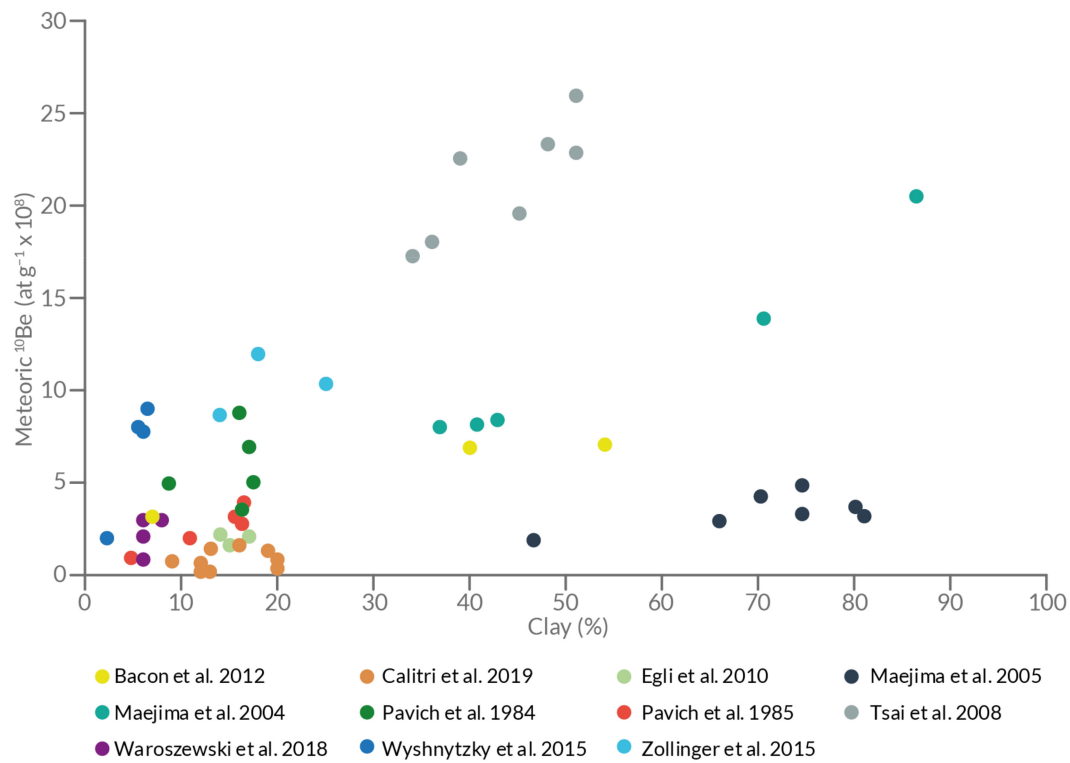
**Figure 2.** Meteoric $^{10}$Be concentrations and clay contents in soils of various environments [2,10–12,15,18,27,33,57,62,63].
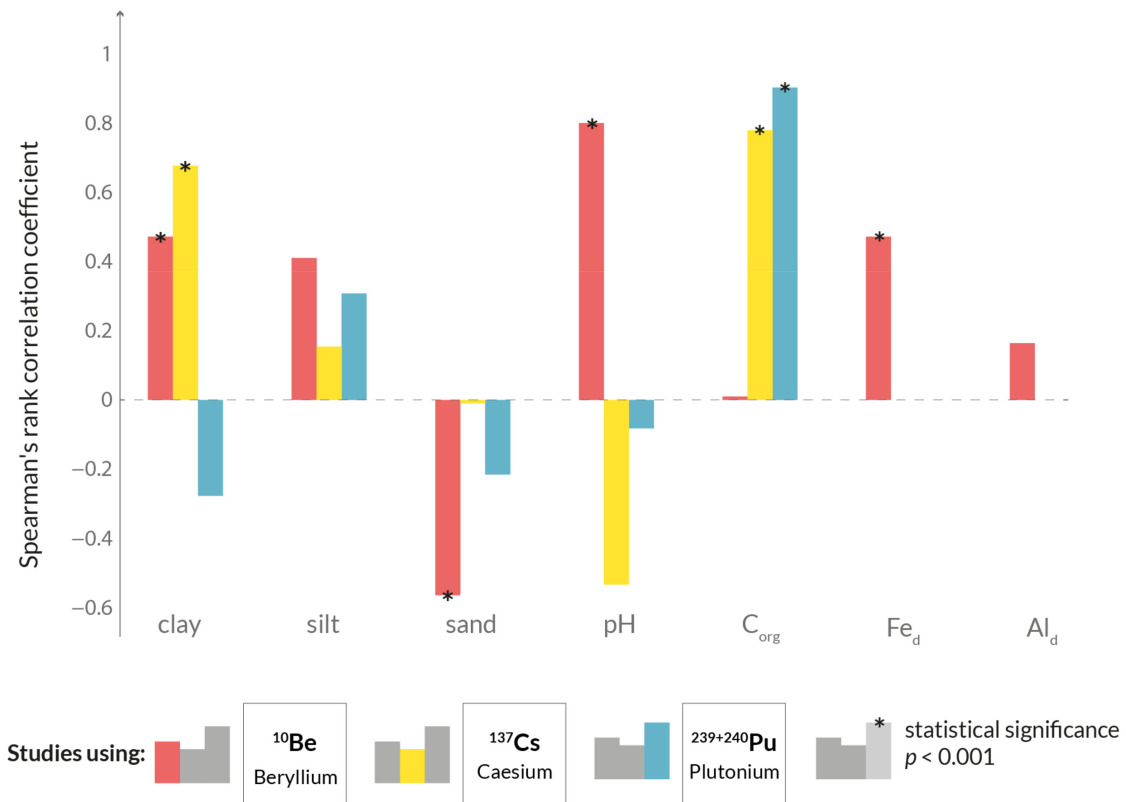


**Figure 3.** Spearman's rank correlation coefficients calculated using data from 27 publications (Table S1) between soil properties of the bulk samples.
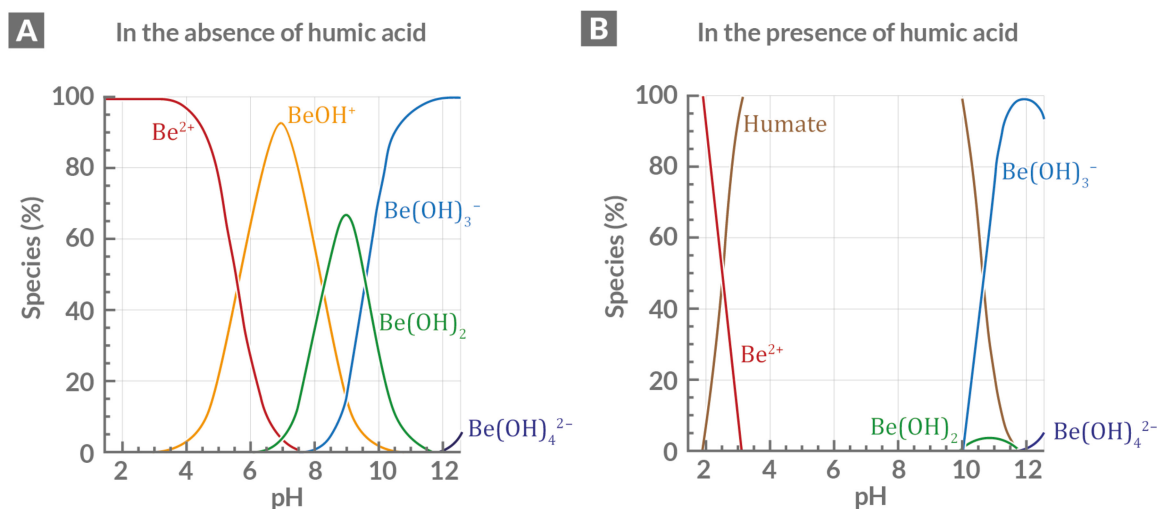
**Figure 4.** Beryllium speciation in aqueous solutions (total concentration of dissolved $^{10}$Be is = 0.02 M) from Takahashi et al. [64]. (**A**) In the absence of organic ("humic") acid and (**B**) in the presence of organic acid (30 mg L$^{-1}$). Reprinted from Geochimica et Cosmochimica Acta, vol. 63, Y. Takahashi, Y. Minai, S. Ambe, Y. Makide, F. Ambe, Comparison of adsorption behavior of multiple inorganic ions on kaolinite and silica in the presence of humic acid using the multitracer technique, pp. 815–836, 1999, with permission from Elsevier.

### 2.3. Origin of Anthropogenic Radionuclides—$^{137}$Cs and $^{239+240}$Pu

Fallout radionuclides (FRNs), such as $^{137}$Cs and $^{239+240}$Pu, are also called anthropogenic radionuclides. They have been distributed across the globe by nuclear weapons fabrication and testing, nuclear power plant accidents and nuclear fuel reprocessing (Figure 1 and Table 1) [17]. The Southern Hemisphere is characterised by a lower total fallout of radionuclides than the Northern Hemisphere, because more atmospheric nuclear testing occurred in the latter one [65]. $^{137}$Cs is characterised by a short half-life of 30.17 y. About 70% of its global fallout has already disappeared through radioactive decay [66]. The plutonium isotopes, however, have a much longer half-life, namely 24,110 y for $^{239}$Pu and 6561 y for $^{240}$Pu. Therefore, they are becoming more popular as a replacement for $^{137}$Cs [66].

### 2.4. Anthropogenic Nuclides in Soils

In soils, plutonium exists in four oxidation states: Pu(III), Pu(IV), Pu(V) and Pu(VI) [49,67]. $^{239+240}$Pu sorption depends on pH and redox conditions. In strongly acidic or anoxic soil conditions, organic compounds reduce Pu(VI) and Pu(V) to immobile Pu(III), which often occurs as an organic complex [49,67–69]. Therefore, $^{239+240}$Pu has a high affinity towards organic matter. Additionally, $^{239+240}$Pu is strongly bound to clay particles, which retain it in the soil [49,70–72]. Our data compilation from 25 soil profiles (Figure 3 and Table S1) showed a strongly positive correlation between $^{239+240}$Pu and organic carbon; however, a strong association with clay was not obvious. $^{239+240}$Pu is a relatively "new" soil erosion tracer. Thus, its sorption–desorption mechanisms in soil are not yet fully understood.

$^{137}$Cs shows a strong affinity towards clay minerals, whereas its affinity towards organic matter is rather low [71,73–75]. Based on data from various environments (*n* = 38 soil profiles), a significant positive correlation between the $^{137}$Cs activity and clay content was found (Figure 3). Additionally, a positive correlation between the $^{137}$Cs activity and organic carbon (*n* = 28) was calculated, but it might be caused by the relatively high SOC content in the samples considered. In general, $^{137}$Cs components are readily soluble in water, although strong adsorption by the clay fraction in soils is highly likely [76]. Thus, the sorption of $^{137}$Cs in the soil system mainly depends on the clay content but also on the pH or the redox conditions. In acidic environments, Cs$^+$ competes with H$^+$ for selective sorption sites, and due to the stronger dissolution of clay minerals in such

environments, the sorption of $^{137}$Cs is lower, whilst under redox conditions, Cs$^+$ competes with NH$_4{}^+$ [74,77,78]. The binding of $^{137}$Cs increases with the increasing pH (Figure 5), because under such conditions, a greater electrostatic attraction of the cation surface occurs; thus, more Cs$^+$ is sorbed onto the negatively charged clay minerals [74]. When the soil organic content is higher than 5%, it starts to outmatch the fixation of Cs$^+$ on clay minerals and becomes available for plant uptake or leaching into deeper soil layers [79,80]. Thus, in peaty or podzolic soils, $^{137}$Cs is considerably more mobile than in other soils [81,82].
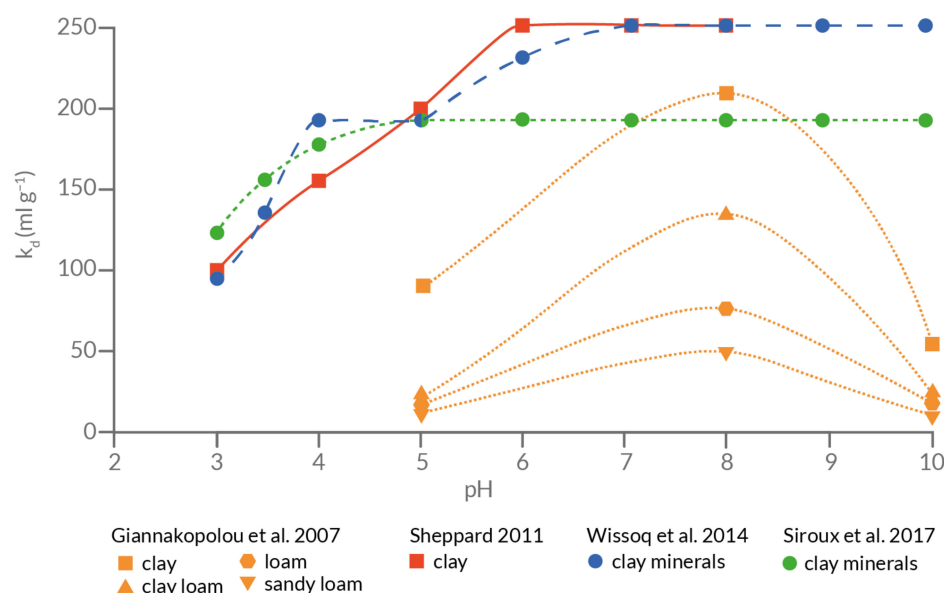


**Figure 5.** Sorption coefficient (k$_d$) of $_{137}$Cs in soils as a function of pH [74,83–85].

## 2.5. Profile Depth Distribution of Meteoric $^{10}$Be, $^{137}$Cs and $^{239+240}$Pu

$^{10}$Be is a useful geochronometer and long-term erosion tracer due to its long half-life (1.387 ± 0.012 Myr), worldwide occurrence and strong binding by fine soil particles [2,33,86]. Adsorbed meteoric $^{10}$Be can be moved along the soil profile because of fine particles translocation via soil water and physical mixing and the percolation of water that may desorb $^{10}$Be and transporting it [2]. In general, the highest content of meteoric $^{10}$Be is measured in horizons having the highest clay contents (Figure 2) [2,10,11,27,37,52,57]. Thus, the distribution of $^{10}$Be within a soil profile in nonacidic conditions as a declining, humped or uniform trend reflects soil evolutionary processes, the degree of surface erosion and soil mass movements [2,18,48,52]. Undisturbed soil profiles are characterised by a declining $^{10}$Be content, with the highest value occurring in the topmost horizons (Figure 6(A1,B1)). Soils on actively eroding hillslopes are also characterised by declining $^{10}$Be contents [48]. However, their highest content is up to one order of magnitude lower compared to noneroded soils (Figure 6(A3,B3)) [48,87]. The highest $^{10}$Be content in subsurface horizons (Figure 6(A2,B2)) is typically found in soils where clay illuviation or intense podzolisation has occurred [11,15,37,57]. Soils that have undergone deep mixing by physical and paedogenic processes or colluvial soils where eroded material from the upper parts of a slope has been deposited (Figure 6 (A4,B4)) are, however, characterised by a uniform $^{10}$Be content [38,48,88]. In cases where the topsoil has a different origin (e.g., due to the addition of aeolian silt) to the underlying horizons, significantly lower $^{10}$Be concentrations occur in the upper part of the soil profile in contrast to the deeper horizons (Figure 6(A5,B5)) [27].
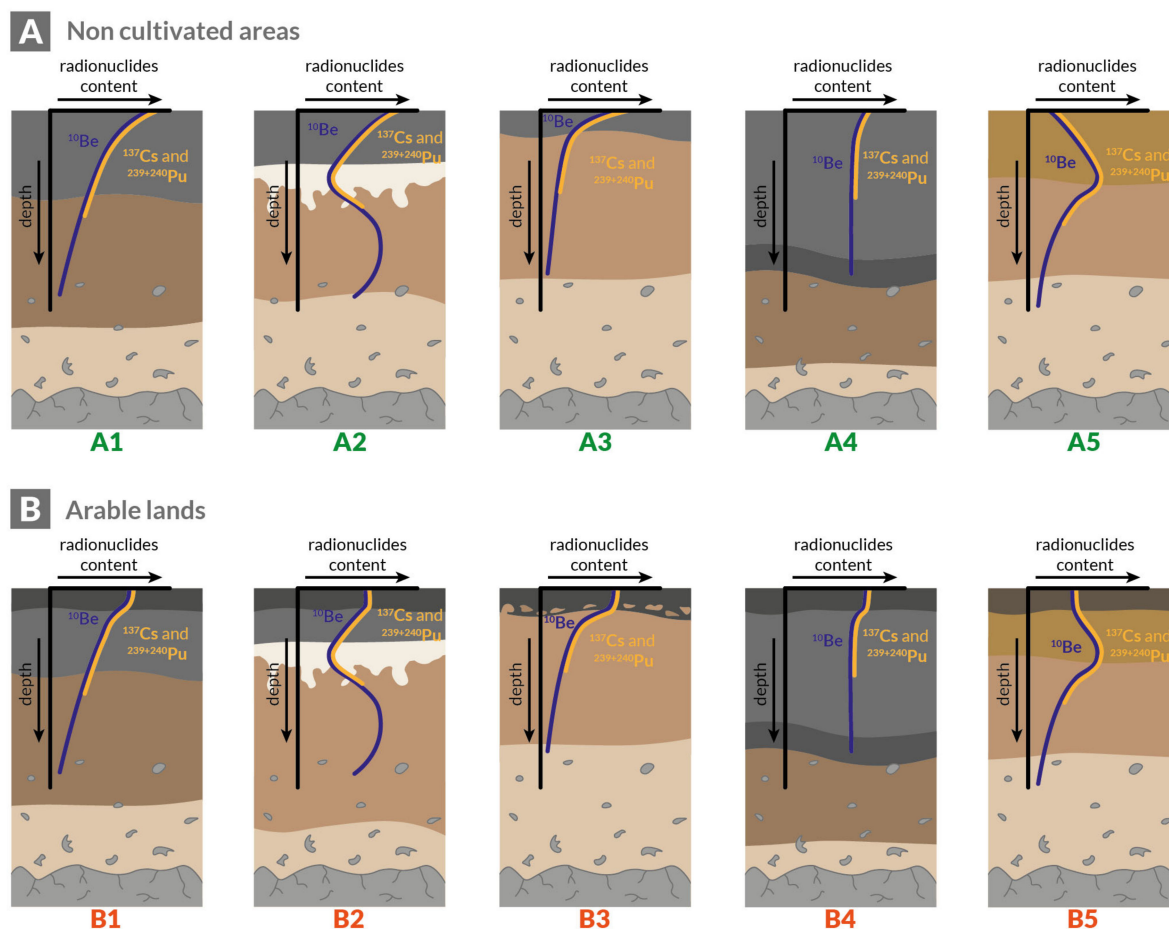
**Figure 6.** Examples of different profile depth distributions of the studied isotopes in ploughed (**A**) and unploughed (**B**) soils: (**A1**,**B1**)—typical distribution, (**A2**,**B2**)—distribution with clay illuviation, (**A3**,**B3**)—distribution under erosion processes, (**A4**,**B4**)—distribution forced by deep mixing and (**A5**,**B5**)—distribution in polygenetic soils.

Additionally, the FRNs from global fallout are strongly adsorbed onto the fine earth fraction in the topsoil [65,89], and their distribution occurs as a result of soil particle movements [65]. Consequently, the profile depth distributions of $^{137}$Cs and $^{239+240}$Pu (Figure 6) are similar to meteoric $^{10}$Be and provide information about soil erosion and accumulation, since they were introduced into the environment [49,90].

## 3. Calculation of Soil Erosion Rates Using Meteoric $^{10}$Be

Most erosion calculations are based on the approaches defined by Lal [91], Egli et al. [15] and Zollinger et al. [19]. However, recently, a few advanced models were proposed to study the distribution of meteoric $^{10}$Be. One of them is the soil–hillslope model (Be2D) that simulates vertical and lateral redistribution of soil and $^{10}$Be along a hillslope and enables insight into processes that influence its transport [92]. The Be2D model considers soil formation, clay translocation, bioturbation and the chemical mobility of $^{10}$Be [92]. Additionally, this model considers soil creep, tillage and water erosion reflecting lateral transport and is fully described in Campforts et al. [92].

Another one is the relatively new LODO (Loss Only, Diffusion Only) model presented by Jeliński et al. [32]. This model simulates $^{10}$Be concentration profiles in soils over time. It considers vertical diffusion and the net soil flux. In the LODO model, the downward migration of $^{10}$Be from the topsoil is modelled as a diffusive process with the depth dependent on diffusivity. It considers that, prior to diffusion, all $^{10}$Be enter the surficial depth increment equally [32].

## 4. Reference Sites and Conversion Models for Anthropogenic Radionuclides

### 4.1. The Importance of Reference Sites

FRN techniques are used to calculate soil erosion or accumulation rates by comparing the total radionuclide inventory per unit area of a reference site with the FRN activity of a study site or by comparing the temporal evolution of the FRN stocks over time (i.e., by revisiting the sites) [49,93]. When the inventory of the study site is lower than that of reference site, this indicates erosion, whereas a higher stock indicates the deposition of soil material [49]. Thus, the choice of reference site plays a crucial role, because inaccurate values ascribed to the reference inventory will lead to underestimation or overestimation of erosion rates [93]. The undisturbed reference site where soil denudation is absent or negligible should be located, e.g., on a flat, well-vegetated, unploughed site [49]. According to Sutherland [94], the isotope content at a reference site can be used to calculate soil erosion if the variance coefficient is <30%. Recently, especially in the case of $^{239+240}$Pu, attention is paid to measure from five up to ten replicate cores per study site or to take a large amount of sample material (around 1–2 kg per sample) and homogenised them to overcome the large sampling number and measurements.

### 4.2. Soil Redistribution Rates

One usually assumes that the source of isotopes is just one, and if not, the percentage deposition from each source has to be known to use the calculation models properly [20,49,95]. This is especially the case with $^{137}$Cs (see Section 4.3). Therefore, the separation of global and Chernobyl fallout may be done by estimating the initial inventory of $^{137}$Cs related to atmospheric nuclear weapon tests. This estimation is based on the approach of Sarmiento and Gwinn [96] and precipitation data [95].

For the estimation of soil erosion and/or deposition rates using $^{137}$Cs and $^{239+240}$Pu, various models like the Proportional Model (PM), Mass Balance Model (MBM), Profile Distribution Model (PDM) and Diffusion and Migration model (DDM) were widely applied [97–103]. Furthermore, a two-dimensional spatial integration of the MBM for $^{137}$Cs was developed [104]. Van Oost et al. [104] described the crucial processes for $^{137}$Cs redistribution that may be independently simulated in this complex approach. Soil mixing and tillage redistribution are modelled by the combination of the spatial distribution of $^{137}$Cs with a displacement distribution, and water erosion is simulated using topographic equations [104]. Additionally, an approach exists that combines the MBM with models estimating the spatial soil redistribution, like WATEM/SEDEM (Water and Tillage Erosion Model/Sediment Delivery Model). Such a combination enables calibrating the parameters of spatial models and a detailed determination of the soil redistribution [31].

In 2016, a new algorithm was proposed—modelling deposition and erosion rates using radio nuclides (MODERN) [49,89]. MODERN is a new concept characterised by several noticeable advantages; it more accurately describes the measured FRN inventory in a soil profile. It does not make any distinct assumptions for the reference site and allows the conversion of isotope inventories into soil gain/loss rates, independent of the type of land use [49].

### 4.3. Radionuclide Ratios

The main assumption of using atmospheric isotopes is that their spatial distributions should be homogeneous [20,95]. However, in Western and Central Europe, the deposition of $^{137}$Cs was rather heterogeneous [49]. Most of the fallout $^{137}$Cs originates from the 1986 Chernobyl incident and not nuclear weapons tests. Additionally, on the East Coast of Honshu Island (Japan), the spatial distribution of $^{137}$Cs fallout is heterogenous due to the Fukushima Daiichi Nuclear Power Plant (FDNPP) accident in 2011 [66]. Thus, the proportion of $^{137}$Cs Chernobyl or FDNPP fallout at reference sites should be known [20]. $^{239+240}$Pu is not present in the volatile fraction of fuel debris from nuclear reactor accidents. Therefore, the Chernobyl $^{239+240}$Pu fallout is more limited to Russia, Ukraine, Belarus, Poland and the Baltic countries [105,106], and the FDNPP $^{239+240}$Pu fallout is mainly centred

around Fukushima Prefecture [107]. Other countries, however, have a homogeneous deposition of $^{239+240}$Pu that originated mainly from the atmospheric nuclear weapons tests conducted in the 1950s and 1960s [17,20]. Therefore, to determine the origin of radionuclides, their ratios are used, because the values of the ratio vary significantly depending on the source [66]. In the Northern Hemisphere, the ratio of $^{240}$Pu/$^{239}$Pu for global fallout ranges from 0.14 to 0.24, with an average of 0.18; for the Chernobyl fallout, the ratios are between 0.37 and 0.41, and for FDNPP, the range is between 0.30 and 0.33 [66,108,109].

## 5. Application in Different Environments in Agricultural and Natural Landscapes

The use of isotopes for the study of soil erosion began in the late 1950s [110]. Since then, $^{10}$Be, $^{137}$Cs and $^{239+240}$Pu isotopes have been used for the estimation of erosion rates at the temporal and spatial scale. However, the rates can drastically differ as a response to land-use changes and modifications in land management. Thus, in this section, we briefly discuss the use of isotopes in different environments (Figures 7 and 8 and Table 2). Erosion rates determined with isotopes are compared with values from RUSLE. Potential problems in their application and how to avoid methodological problems are addressed (Table 3). Additionally, Mabit et al. [111] pointed out that FRNs should be used for studying soil redistribution within watersheds, the conversion models used should be improved and a conjunctive use of isotopes that cover different timescales provide more information about a study site. Below, we present whether these points are met in the current studies by analysing 83 soils from alpine sites, 35 from loess deposits, 28 from moraine landscapes, 35 from coral reef terraces and Mediterranean areas and 17 soils from the tropics (Figure 7).
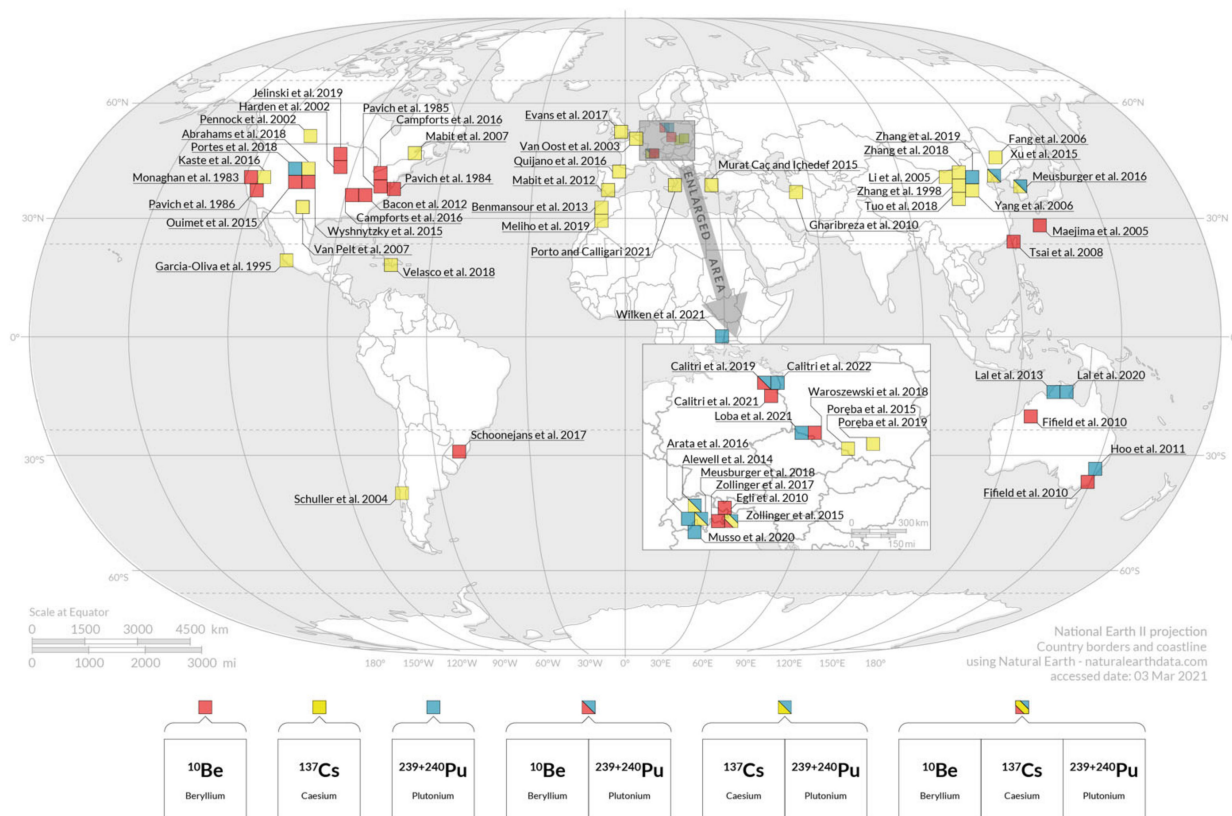


**Figure 7.** Worldwide isotopic studies (meteoric $^{10}$Be, $^{137}$Cs and $^{239+240}$Pu) dealing with the soil redistribution rates [2,11,12,15,17–30,32–36,38–42,57,60,62,63,66,79,87,89,92,95,104,112–130].
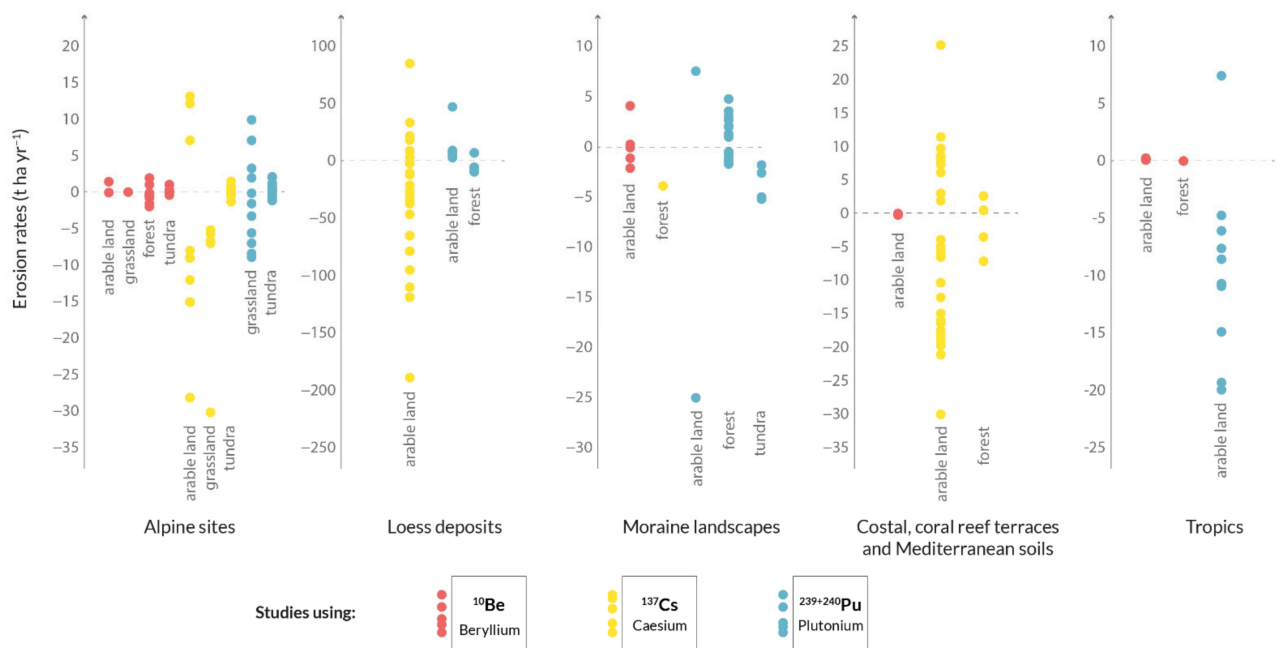
**Figure 8.** Compilation of published soil erosion rates determined with meteoric $^{10}$Be, $^{137}$Cs and $^{239+240}$Pu in different environments. Negative values = erosion and positive values = accumulation.

**Table 2.** Published soil erosion rates based on various isotopes and conversion models (only publications considered where both were available: isotope content and calculation of the soil redistribution rates).

| No | Author | Location | Soil Texture | Number of Profiles | Land Use | Soil Erosion Rates (t ha$^{-1}$ y$^1$) | | | |
|---|---|---|---|---|---|---|---|---|---|
| | | | | | | Meteoric $^{10}$Be | $^{137}$Cs | $^{239+240}$Pu | (R)USLE *** |
| 1 | Maejima et al. [11] | Coral reef terraces, Southwest Japan | C, SiC, CL | 9 | Arable land | −0.098 to −0.31 [a,*] | - | - | n.d. ** |
| 2 | Tsai et al. [12] | Fluvial terraces, Taiwan | C, SiC, CL | 3 | n.d. ** | −0.125 to −0.263 [a] | - | - | n.d. ** |
| 3 | Egli et al. [15] | Swiss and Italian Alps | LS, SL | 6 | Mixed forest/alpine grassland | −0.6 to −2.50 [a] −0.03 to −0.6 [b] | - | - | −0.1 to −0.5 [131] |
| 4 | Fifield et al. [127] | Fingerpost Hill, Burra Creek, NW and SE Australia | n.d. ** | 13 | Forest and Pasture | −0.03 to −0.19 [a] | | | −0.1 to −5.0 [132] |
| 5 | Campforts et al. [92] | Susquehanna Shale Hills Observatory, USA | n.d. | n.d. ** | Arable land | −0.10 to 1.37 [c] | | | n.d. |
| 6 | Zollinger et al. [19] | Swiss Alps | LS, SL | 18 | Alpine grassland | −0.34 to −1.29 [a] −0.08 to 1.8 [b] | - | - | −1.0 to −0.3 [131] |

**Table 2.** *Cont.*

| No | Author | Location | Soil Texture | Number of Profiles | Land Use | Soil Erosion Rates (t ha$^{-1}$ y$^1$) | | | |
|---|---|---|---|---|---|---|---|---|---|
| | | | | | | Meteoric $^{10}$Be | $^{137}$Cs | $^{239+240}$Pu | (R)USLE *** |
| 7 | Schoonejans et al. [25] | Critical Zone Observatory, Southern Brazil | n.d. ** | 3 | Subtropical forest | −0.33 to −0.42 [d] −0.05 to −0.06 [e] | - | - | n.d. |
| 8 | Waroszewski et al. [27] | Karkonosze Mountains, Poland | SL, SiL | 5 | Mountain forest | −1.3 to −6.4 [f] −0.8 to −2.0 [g] | - | - | −2.0 to −5.0 [133] |
| 9 | Jelinski et al. [32] | West-Central Minnesota, USA | L | 5 | Arable land | −0.06 to 4.13 [h] | n.d. | | n.d. |
| 10 | Zhang et al. [39] | Ansai, China | SiL | 9 | Arable land | | −65.0 to 110.0 [i] | - | −50 to −80 [134] |
| 11 | Van Oost et al. [104] | Huldenberg, central Belgium | SiL | n.d. ** | Arable land | | −10.3 to 9.0 [j] | - | −0.5 to −1.0 [133] |
| 12 | Schuller et al. [115] | Coastal Mountain range of the 9th Region of Chile | n.d. ** | 6 | Arable land | | −28.0 to 12.0 [i] | - | n.d. |
| 13 | Fang et al. [125] | Jilin Province, China | CL | 5 | Arable land | | −26.43 to 27.28 [k] −37.63 to 34.33 [i] | - | −45.0 to −4.0 [135] |
| 14 | Yang et al. [126] | Shaanxi Province, China | SiL | 197 | Forest and arable land | | −25.0 to 150.0 [i,m] | - | −23.1 [135] |
| 15 | Mabit et al. [28] | Boyer River watershed, Canada | SL, SCL | 412 | Arable land | - | −9 to 6.4 [i] | - | −3.0 [28] |
| 16 | Mabit et al. [29] | Montefrio, Spain | CL | 8 | Arable land | | −19.0 to 25.0 [i] | - | −10 to −20 [133] |
| 17 | Benmansour et al. [118] | Marchouch, Morocco | C | 45 | Arable land | | −4.0 to −30.0 [i] | - | −4.0 to −56.0 [118] |
| 18 | Murat Sac and Ichedef [120] | Salihi Region, Western Turkey | n.d. ** | 4 | Arable land | - | −21.1 to 11.3 [i] −9.6 to 19.4 [k] | - | n.d. |
| 19 | Poręba et al. [38] | Świerklany, South Poland | SiL | 4 | Arable land | - | −26.7 to 85.1 [i] | - | −10.0 to −20.0 [133] |
| 20 | Quijano et al. [117] | Ebro Basin, Spain | n.d. | 156 | Arable land | | −19.8 to 7.4 [i] | - | −10.0 to −20.0 [133] |
| 21 | Velasco et al. [24] | Forêts des Pins, Haiti | C | 12 | Arable land | - | −23 to 71 [l] | - | −20 to −50 [136] |
| 22 | Tuo et al. [36] | Chinese Loess Plateau | SL | 7 | Arable land | - | −21.39 to −37.31 [i] | - | −23.1 [137] |
| 23 | Poręba et al. [95] | Biedrzykowice, South Poland | SiL | 4 | Arable land | - | −4.9 to 39.9 [i, k] | - | −10.0 to −20.0 [133] |
| 24 | Meliho et al. [30] | Ourika Watershed, High Atlas of Morocco | SL, L | 33 | Arable land and forest | - | −32.23 to −0.06 [i] −11.42 to 2.27 [m] | - | up to −45.0 [138] |
| 25 | Gharibreza et al. [124] | Golestan Province, Iran | SiL, SiC | 93 | Arable land and forest | - | −10 to −35.9 [i] | - | up to −70.0 [139] |

**Table 2.** *Cont.*

| No | Author | Location | Soil Texture | Number of Profiles | Land Use | Soil Erosion Rates (t ha⁻¹ y¹) | | | |
|----|--------|----------|--------------|--------------------|----------|--------------|--------|--------|--------|
| | | | | | | Meteoric $^{10}$Be | $^{137}$Cs | $^{239+240}$Pu | (R)USLE *** |
| 26 | Xu et al. [140] | Liaodong Bay, Northeast China | n.d. | 6 | Arable land and uncultivated land with low vegetation cover | - | −14.0 to −42.5 i | −20.3 to −72.0 j | n.d. |
| 27 | Meusburger et al. [89] | headwater catchment of Lake Soyang, South Korea | SL | 25 | Forest and arable land | - | −23.8 to 2.9 m | −17.5 to 3.6 l | −30.6 to −54.8 [141] |
| 28 | Meusburger et al. [20] | Swiss Central Alps | LS, SL | 14 | Alpine grassland | - | −5.2 to −6.7 l | −3.3 to −7.0 o | −2.0 to −12.0 [142] |
| 29 | Lal et al. [22] | Daly river basin, Northern Australia | n.d. | 6 | Arable land | - | - | −7.5 to −19.5 k; −8.5 to −19.7 i | −10.0 to −50.0 [132] |
| 30 | Alewell et al. [17] | Swiss Central Alps | LS, SL | 44 | Alpine grassland | - | - | −8.9 to 8.3 m; −1.9 to 7.0 k; −0.2 to −16.4 n | −2.0 to −12.0 [142] |
| 31 | Arata et al. [129] | Swiss Central Alps | LS, SL | 5 | Mountain grassland | - | - | −8.4 to 9.8 o | −2.0 to −12.0 [142] |
| 32 | Portes et al. [21] | Central Rocky Mountains, USA | LS, SL | 3 | Alpine tundra/forest | - | - | −2.60 to −5.20 k,m | n.d. |
| 33 | Zhang et al. [121] | Gansu Province, China | SiL | 6 | Forest (before agriculture) | | - | −9.4 to 7.2 i | −23.1 [137] |
| 34 | Lal et al. [23] | The Daily River Catchment, Northern Australia | L | 3 | Pasture, mahogany and peanut plantations | - | - | −8.4 to 7.2 i | −10 to −50 [132] |
| 35 | Loba et al. [40] | Trzebnica Hills, Southwest Poland | SiL, L | | Arable land | | | −1.17 to 10.93 o | −5.0 to −10.0 [133] |
| 36 | Zollinger et al. [18] | Eastern Swiss Alps | LS, SL | 19 | Alpine tundra/natural forest | −0.40 to 0.04 b | −1.35 to 1.41 m | −1.20 to 2.04 m | −1.0 to −2.0 [131] |
| 37 | Calitri et al. [33] | Uckermark Region, Northeast Germany | SL, L | 3 | Arable land | −2.11 to 0.26 b | - | −0.25 to 7.6 m | up to −0.5 [133] |

* Negative values mean erosion, positive deposition. ** No data. *** Authors are given in the brackets. Soil texture: SL—sandy loam, LS—loamy sand, L—loam, SiL—silt loam, SCL—sandy clay loam, SiC—silty clay, CL—clay loam and C—clay. Models: ᵃ Steady-state approach, ᵇ non-steady-state approach, ᶜ Be2D model, ᵈ not-corrected values, ᵉ corrected values, ᶠ assuming that the uppermost horizon has the same origin as the underlying soil, ᵍ the uppermost horizon is not considered due to its different origin, ʰ integration of Be2D and LODO, ⁱ mass balance model, ʲ integration of mass balance and spatial models, ᵏ proportional model, ˡ diffusion and migration model, ᵐ profile distribution model, ⁿ inventory method and ᵒ MODERN.

**Table 3.** Summary of some main potential problems in applying isotopes as a soil tracer and possibilities for overcoming them.

| Environment | Land Use | Difficulties | Solutions |
| --- | --- | --- | --- |
| Alpine sites, Loess areas | Grasslands, Forests, Arable lands | Heterogenous fallout of $^{137}$Cs (Nuclear weapons tests and nuclear power plants fallout), which affects the calculation of soil erosion rates. | To overcome this limitation, both sources of $^{137}$Cs have to be taken into account in the calculation model. The separation of global fallout from e.g., the Chernobyl fallout may be done by estimating the initial inventory of $^{137}$Cs (described in Poręba et al. [95]) or by the determination of $^{239+240}$Pu/$^{137}$Cs activity ratios at reference sites (described in Meusburger et al. [20,143]). |
| Coral reef and fluvial terraces, Alpine sites | Grasslands, Forests, Arable lands | When meteoric $^{10}$Be is used, the erosion/deposition rates obtained with the model of Lal [91], sometimes may raise doubts. Especially in soils exhibiting clay illuviation or podzolisation. | Application of different models, e.g., proposed by Egli et al. [15], Be2D model [92] and LODO [32] |
| Tropics | Arable lands | When soil is cultivated with traditional manual tillage practices, features of significant tillage mixing does not occur. Thus, conversion models for cultivated sites cannot be used. | A conversion model developed for undisturbed soils has to be applied [24]. |
| Alpine sites | Forests | Cover beds or different overlaying parent materials for soil development exist. The topsoil, for example, may have aeolian silt admixture, whereas this is not the case for the subsoil. The interpretation of long-term erosion rates may be hampered. | Calculation of erosion rates with and without considering the topsoil may give indications about the range of results [27]. |
| Acidic soils | Forests | In acidic soils, the considered isotopes may in part be solubilised and, thus, be leached. | Determination of a potential loss of meteoric $^{10}$Be from the parent material, using chemical mass losses of stable $^{9}$Be in a regolith profile [25,62]. The concepts and models for $^{137}$Cs and $^{239+240}$Pu under acidic conditions still need to be improved. |

*5.1. Alpine Sites*

Although, there are certain limitations in the application of the discussed isotopes at Alpine sites, they have been widely used to determine soil redistribution rates [15–19,27,92,129,130,144,145]. For example, Alewell et al. [17] employed $^{239+240}$Pu and $^{137}$Cs as tools in measuring soil erosion in mountainous grasslands in the Swiss Alps. At such sites, the distribution of $^{137}$Cs was chiefly due to the fallout from the Chernobyl accident. This incident occurred at a time when the mountains were still snow-covered. Following snowmelt, the spatial distribution of $^{137}$Cs became very patchy, because part of it was lost due to the overland surface flow, whereas, at sites that had been snow-free, the $^{137}$Cs remained and accumulated in the soil. The spatial distribution of $^{239+240}$Pu, however,

was not affected by the nuclear accident. Therefore, the erosion rates were determined using $^{239+240}$Pu (Table 2). The application of $^{137}$Cs at such Chernobyl-affected sites is, however, still possible. To overcome this limitation, Meusburger et al. [20] determined the $^{239+240}$Pu/$^{137}$Cs activity ratios at the reference sites. The calculation of this ratio provided information about the relative influence of the global versus Chernobyl deposition and allowed the consideration of two $^{137}$Cs sources by a using conversion model. The values of the $^{239+240}$Pu/$^{137}$Cs activity ratios increased with the soil depth, indicating the predominant origin of the $^{137}$Cs in the topsoil being Chernobyl, while the deeper layers were characterised by a higher proportion of the $^{137}$Cs from global fallout. Therefore, the average Chernobyl contribution was estimated to be 75%, which was used to convert the $^{137}$Cs inventories (Table 2), and the obtained results were in the range of those determined with RUSLE [131] (Table 2).

The soil erosion rates using $^{137}$Cs and $^{239+240}$Pu were also determined in the Lake Soyang catchment, which has a total area of 65 km$^2$ [89]. The rates agree well with data from RUSLE [141]. The calculation model is crucial for the interpretation of long-term erosion rates based on meteoric $^{10}$Be at Alpine sites. As discussed by Zollinger et al. [19] and Egli et al. [15], an approach using steady-state conditions gives unreliable results and does not detect deposition processes. In addition, the interpretation of meteoric $^{10}$Be data becomes difficult in soils developed from heterogenous parent materials. This problem was addressed by Waroszewski et al. [27], where a thin aeolian silt drape overlayed periglacial mica schist deposits; thus, two calculations were used and compared to estimate the erosion rates in mountainous forests. The first based on the assumption that the uppermost horizon had the same origin as the underlying layers, and the second did not consider the uppermost horizon due to its different origin. Version 1 overestimated the erosion rates, while version 2 produced erosion values (Table 2) that seemed more plausible for this mountainous region. The better suitability of the second version was also supported by RUSLE data (Table 2).

Recently, using a combination of isotopes that cover different intervals of time (e.g., $^{239+240}$Pu and $^{10}$Be) has been applied. This can help in deciphering processes over different timescales. It may shed light onto changes of soil redistribution caused by evolving environmental settings or anthropogenic forcing and allow for the comparison of different time ranges. For instance, Zollinger et al. [19] showed that the short- to mid-term soil redistribution rates in the alpine tundra are dramatically higher than the long-term rates (covering a period of ~15 kyr). This has been mainly caused by climate warming and melting of the permafrost, which has distinctly increased soil redistribution over the last few decades.

### 5.2. Loess Deposits

Loess deposits are very susceptible to erosion processes [124,139,146–149]. Thus, isotopic techniques were widely applied in such landscapes [36,38,39,95,104,121,126,150]. Poręba et al. [38,95] applied $^{137}$Cs measurements to a loess colluvium to interpret soil erosion in a Polish loess area under agriculture use (arable lands). In this case, about 45–90% of $^{137}$Cs derived from the Chernobyl accident. When taking this into account, the erosion rates were in a typical range for loess environments, as shown by RUSLE (Table 2). Other results showed, by using $^{239+240}$Pu, that the soil erosion rates of loess landscapes of Southwestern Poland are often much higher than tolerable rates but still in the range of values from RUSLE [40]. For the Chinese Loess Plateau, Zhang et al. [39] showed that soil erosion determined using $^{137}$Cs is considerably lower than the modelled rates using the RUSLE model or sediment yields. This issue was explained by the simulation errors and the effect of the topography. Additionally, in arable areas of the Chinese Loess Plateau, $^{137}$Cs was involved to determine wind erosion by subtracting the water erosion from the total erosion calculated using $^{137}$Cs [36,123,151]. However, such an approach can cause some uncertainty. The RUSLE model, which is used to calculate water erosion, may underestimate or overestimate erosion rates [36,151]. Thus, the issue of determining wind erosion

with isotopes definitely requires more research. In loess landscapes, the methodological combination of soil redistribution rates based on ^{137}Cs measurements with spatial soil erosion models was applied in forests and arable lands [104,126]. Recently, [239+240]Pu and ^{137}Cs were used for the assessment of rehabilitation effectiveness at sites that were used in the past for agriculture and now are afforested or are grasslands [121,124,127,134]. Examples showing the effect of changes in a tillage system on erosion rates in loess landscapes are still scarce.

### 5.3. Moraine Landscapes

In moraine landscapes, radioisotopes may help to decipher the evolution of soil erosion rates with soil development. Portes et al. [21], by using [239+240]Pu, showed that soil erosion rates in forests and the tundra on moraine hillslopes have strongly decreased over time. Both applied models—the profile distribution model [98,100] and the inventory model [22]—detected the same trend. The application of [239+240]Pu in forests of such landscapes may provide information if the erosion in a studied area is recent or ancient, as presented by Calitri et al. [34]. The combination of [239+240]Pu (last few decades) and meteoric [10]Be (integration over millennia) in arable lands often confirms that the intensification of agriculture in recent decades has strongly influenced soil redistribution rates [33]. Moreover, recent investigations of Jelinski et al. [32] exhibited that natural and anthropogenic soil redistribution rates can be discerned when meteoric [10]Be is combined with the LODO, Be2D and WaTEM models.

Some investigations, however, did not focus on the calculation of soil erosion and considered only isotope inventories [2,35]. Ouimet et al. [35] presented the spatial and temporal variations of meteoric [10]Be inventories in moraines and fluvial terraces, which allowed to identify specific slope processes. Soil erosion seemed to have occurred even at the older sites (>90 ka), whereas the younger sites (15–21 ka) exhibited higher [10]Be inventories, indicating the dynamic aspects of [10]Be deposition, like snow drift that caused spatial variations in measured inventories at individual sites.

### 5.4. Coastal and Coral Reef Terraces and Mediterranean Soils

Isotopes were also applied in soils on coral reef, coastal and fluvial terraces [11,12,35,60,113,120] and Mediterranean landscapes [29–31,118]. Maejima et al. [11] and Tsai et al. [12] applied (meteoric) [10]Be to the soils of uplifted coral reef terraces in Southwestern Japan and in fluvial terraces in Taiwan, respectively. These cases showed the importance of the calculation model for the determination of soil erosion rates. In both publications, the mathematical model of Lal [91] was used. Therefore, processes such as eluviation/illuviation or vertical mixing were not considered in the model, which resulted in an overestimation of the soil erosion rates.

Radioisotopes are suitable tracers of soil erosion rates in such environments [35,60]. For instance, Meliho et al. [30] applied ^{137}Cs to determine the erosion on terraces with different land uses (forestry and agriculture) in the High Atlas (Ourika watershed) of Morocco, whereas Mabit et al. [29] and Quijano et al. [31] applied radioisotopes to study soil erosion alone or in combination with spatial models in Mediterranean landscapes. The obtained results were reliable, because they lie in the range of data provided by RUSLE (Table 2; Panagos et al. [133,138]).

### 5.5. Tropics

Radioisotopes have been widely used in the tropics [22,23,79,127,128] and comparable with results from USLE model [132,136]. Lal et al. [23] applied [239+240]Pu to analyse soil losses and gains in the wet–dry tropics of Northern Australia on three major land-use types (grazing fields, mahogany and peanut plantation). Wilken et al. [26] demonstrated that pristine forests show no indication of soil redistribution based on [239+240]Pu along topographical gradients. They, however, have measured tremendously high soil erosion and sedimentation rates up 87 t ha$^{-1}$ y$^{-1}$ during the last 55 years. Hoo et al. [128] also

used [239]Pu to determine the recent soil erosion rates at the scale of a Canberra water supply catchment of a few hundred km$^2$ in a fire-ravaged area. Here, erosion and water quality are tightly interconnected. Fifield et al. [127] combined meteoric [10]Be and ^{137}Cs to compare the long- and medium-term soil erosion and production rates. The authors showed that modern soil loss is considerably higher than soil production. [137]Cs also traced erosion processes on hillslopes in Haiti, where tillage is performed with traditional manual tools. Thus, cultivated sites did not exhibit any evidence of significant tillage mixing, and it was not possible to apply a standard conversion model for cultivated soils. Consequently, a conversion model developed for undisturbed sites had to be used to calculate the soil erosion rates, which seemingly provided reliable results [24].

*5.6. Acidic Soils*

Under acidic conditions, the discussed isotopes may occur in mobile forms, and they may be transported to the saprolite and/or lost through leaching [52,59,62,74,152]. To overcome this limitation for meteoric [10]Be, Bacon et al. [62] proposed to use the stable isotope [9]Be that is mobilised from the parent material through weathering to determine the potential loss of meteoric [10]Be [25]. This approach is based on the chemical mass losses of [9]Be in a regolith profile being used to constrain the chemical depletion of [10]Be. Adding chemical losses of [9]Be to the measured [9]Be inventory and assuming that [9]Be and meteoric [10]Be behave similarly in the regolith, the reactive [9]Be fractions are positively related to the [10]Be concentrations. Therefore, the ratio between the corrected and measured [9]Be concentrations enables a correction of the [10]Be concentrations, so that erosion rates can be calculated. Additionally, in acidic environments such as forests, the Be2D model, which considers meteoric [10]Be translocation within a soil profile, was applied, and the results seemed reasonable [92].

## 6. Conclusions and Outlook

Meteoric [10]Be, ^{137}Cs and [239+240]Pu are useful tracers of soil redistribution. They have been applied in different environments, such as moraines, loess landscapes, alpine sites, coastal and coral reef terraces, Mediterranean soils, tropics, acidic soils and forest soils and used as forests, grasslands and arable lands. The results determined with isotopes were in a good agreement with the values from RUSLE, which proves their usefulness as soil erosion tracers. Meteoric [10]Be allows the calculation of long-term redistribution rates (often since the start of soil formation), while ^{137}Cs and [239+240]Pu give possibility to calculating the medium-term (decades) rates. The application of ^{137}Cs, however, has increasing limitations caused by its short half-life and its heterogeneous distribution in European soils owing to the Chernobyl nuclear accident. Thus, [239+240]Pu has been suggested as a promising alternative. Its high precision and increasing application have indicated its success.

When using these isotopes, a crucial issue is selecting the most suitable conversion model for calculating the soil redistribution rates. For meteoric [10]Be, the most popular models are those proposed by Lal [91] and Egli et al. [15]; however, the latter appears to work better, because it assumes that soils are an open system. New models such as LODO with Be2D provide insights into the natural and anthropogenic soil redistribution rates. For ^{137}Cs and [239+240]Pu, the mass balance, diffusion and migration, profile distribution models and inventory method are often used, whereas MODERN is a recently developed model that stimulates the stock and the FRN profile distribution.

When using [239+240]Pu and ^{137}Cs, the choice of a reference profile is crucial, as the results of sites exhibiting soil redistribution are referenced. Choosing an unrepresentative (disturbed and eroded) reference profile will lead to under- or overestimation of these rates.

Many examples have proved the usefulness of these isotopes in estimating the soil redistribution rates. There are, however, also several limitations with these isotopic methods, although solutions exist for some of them. For example, the distribution of ^{137}Cs may not be homogeneous. In such cases, [239+240]Pu may be helpful in correcting any bias. Likewise,

in deeply weathered and acidic soils, losses of the inventory of $^{10}$Be may be corrected by using $^{9}$Be.

Moreover, the simultaneous application of $^{10}$Be and $^{137}$Cs and/or $^{239+240}$Pu enables tracing back changes in the soil erosion rates over time. It has been shown that global warming has accelerated the soil redistribution rates in Alpine regions and on agriculture land. Using a combination of several isotopes at the same study sites enables cross-checking whether the obtained results are comparable and, therefore, reliable. This kind of approach was presented by Mabit et al. [111] as a challenge and necessity in the use of isotopes.

Isotopic tools are still underexplored in soils, but they could be increasingly applied under different agroecological conditions, with soil redistribution rates being quantified over decades to millennia. Still, several gaps in the knowledge about soil redistribution exists, e.g., in loess areas under different tillage systems or applying isotopes in larger scales like watersheds. The determination of wind erosion and the application of new calculation models are additional challenges.

# References

1. Dethier, D.P.; Birkeland, P.W.; McCarthy, J.A. Using the accumulation of CBD-extractable iron and clay content to estimate soil age on stable surfaces and nearby slopes, Front Range, Colorado. *Geomorphology* **2012**, *173–174*, 17–29. [CrossRef]
2. Wyshnytzky, C.E.; Ouimet, W.B.; McCarthy, J.; Dethier, D.P.; Shroba, R.R.; Bierman, P.R.; Rood, D.H. Meteoric $^{10}$Be, clay, and extractable iron depth profiles in the Colorado Front Range: Implications for understanding soil mixing and erosion. *Catena* **2015**, *127*, 32–45. [CrossRef]
3. Dixon, J.L.; von Blanckenburg, F. Soils as pacemakers and limiters of global silicate weathering. *C. R. Geosci.* **2012**, *344*, 597–609. [CrossRef]
4. Frank, M.; Schwarz, B.; Baumann, S.; Kubik, P.W.; Suter, M.; Mangini, A. A 200 kyr record of cosmogenic radionuclide production rate and geomagnetic field intensity from $^{10}$Be in globally stacked deep-sea sediments1. *Earth Planet. Sci. Lett.* **1997**, *149*, 121–129. [CrossRef]
5. Simon, Q.; Suganuma, Y.; Okada, M.; Haneda, Y. High-resolution $^{10}$Be and paleomagnetic recording of the last polarity reversal in the Chiba composite section: Age and dynamics of the Matuyama–Brunhes transition. *Earth Planet. Sci. Lett.* **2019**, *519*, 92–100. [CrossRef]
6. Wagner, G.; Beer, J.; Masarik, J.; Muscheler, R.; Kubik, P.W.; Mende, W.; Laj, C.; Raisbeck, G.M.; Yiou, F. Presence of the Solar de Vries Cycle (~205 years) during the Last Ice Age. *Geophys. Res. Lett.* **2001**, *28*, 303–306. [CrossRef]
7. Wagner, G.; Laj, C.; Beer, J.; Kissel, C.; Muscheler, R.; Masarik, J.; Synal, H.-A. Reconstruction of the paleoaccumulation rate of central Greenland during the last 75 kyr using the cosmogenic radionuclides $^{36}$Cl and $^{10}$Be and geomagnetic field intensity data. *Earth Planet. Sci. Lett.* **2001**, *193*, 515–521. [CrossRef]
8. Frank, M.; Backman, J.; Jakobsson, M.; Moran, K.; O'Regan, M.; King, J.; Haley, B.A.; Kubik, P.W.; Garbe-Schönberg, D. Beryllium isotopes in central Arctic Ocean sediments over the past 12.3 million years: Stratigraphic and paleoclimatic implications. *Paleoceanography* **2008**, *23*, 1–12. [CrossRef]
9. Dannhaus, N.; Wittmann, H.; Krám, P.; Christl, M.; von Blanckenburg, F. Catchment-wide weathering and erosion rates of mafic, ultramafic, and granitic rock from cosmogenic meteoric $^{10}$Be/$^{9}$Be ratios. *Geochim. Cosmochim. Acta* **2018**, *222*, 618–641. [CrossRef]
10. Maejima, Y.; Matsuzaki, H.; Nakano, C. $^{10}$Be concentrations of Red soils in Southwest Japan and its possibility of dating. *Nucl. Instrum. Methods Phys. Res. Sect. B Beam Interact. Mater. At.* **2004**, *223–224*, 596–600. [CrossRef]

11. Maejima, Y.; Matsuzaki, H.; Higashi, T. Application of cosmogenic [10]Be to dating soils on the raised coral reef terraces of Kikai Island, southwest Japan. *Geoderma* **2005**, *126*, 389–399. [CrossRef]

12. Tsai, H.; Maejima, Y.; Hseu, Z.Y. Meteoric [10]Be dating of highly weathered soils from fluvial terraces in Taiwan. *Quat. Int.* **2008**, *188*, 185–196. [CrossRef]

13. Hao, Y.; Xu, Y.; Pan, S.; Song, X.; Zhang, K.; Guo, H.; Gu, Z. Sources of plutonium isotopes and ^{137}Cs in coastal seawaters of Liaodong Bay and Bohai Strait, China and its environmental implications. *Mar. Pollut. Bull.* **2018**, *130*, 240–248. [CrossRef]

14. Dong, W.; Zheng, J.; Guo, Q. Particle-size speciation of Pu isotopes in surface soils from Inner Mongolia (China) and its implications for Asian Dust monitoring. *Appl. Radiat. Isot.* **2017**, *120*, 133–136. [CrossRef] [PubMed]

15. Egli, M.; Brandová, D.; Böhlert, R.; Favilli, F.; Kubik, P.W. [10]Be inventories in Alpine soils and their potential for dating land surfaces. *Geomorphology* **2010**, *119*, 62–73. [CrossRef]

16. Konz, N.; Prasuhn, V.; Alewell, C. On the measurement of alpine soil erosion. *Catena* **2012**, *91*, 63–71. [CrossRef]

17. Alewell, C.; Meusburger, K.; Juretzko, G.; Mabit, L.; Ketterer, M.E. Suitability of [239+240]Pu and ^{137}Cs as tracers for soil erosion assessment in mountain grasslands. *Chemosphere* **2014**, *103*, 274–280. [CrossRef]

18. Zollinger, B.; Alewell, C.; Kneisel, C.; Meusburger, K.; Brandová, D.; Kubik, P.; Schaller, M.; Ketterer, M.; Egli, M. The effect of permafrost on time-split soil erosion using radionuclides (^{137}Cs, [239+240]Pu, meteoric [10]Be) and stable isotopes ($\delta^{13}$C) in the eastern Swiss Alps. *J. Soils Sediments* **2015**, *15*, 1400–1419. [CrossRef]

19. Zollinger, B.; Alewell, C.; Kneisel, C.; Brandová, D.; Petrillo, M.; Plötze, M.; Christl, M.; Egli, M. Soil formation and weathering in a permafrost environment of the Swiss Alps: A multi-parameter and non-steady-state approach. *Earth Surf. Process. Landf.* **2017**, *42*, 814–835. [CrossRef]

20. Meusburger, K.; Porto, P.; Mabit, L.; La Spada, C.; Arata, L.; Alewell, C. Excess Lead-210 and Plutonium-239+240: Two suitable radiogenic soil erosion tracers for mountain grassland sites. *Environ. Res.* **2018**, *160*, 195–202. [CrossRef]

21. Portes, R.; Dahms, D.; Brandová, D.; Raab, G.; Christl, M.; Kühn, P.; Ketterer, M.; Egli, M. Evolution of soil erosion rates in alpine soils of the Central Rocky Mountains using fallout Pu and $\delta^{13}$C. *Earth Planet. Sci. Lett.* **2018**, *496*, 257–269. [CrossRef]

22. Lal, R.; Tims, S.G.; Fifield, L.K.; Wasson, R.J.; Howe, D. Applicability of [239]Pu as a tracer for soil erosion in the wet-dry tropics of northern Australia. *Nucl. Instrum. Methods Phys. Res. Sect. B Beam Interact. Mater. At.* **2013**, *294*, 577–583. [CrossRef]

23. Lal, R.; Fifield, L.K.; Tims, S.G.; Wasson, R.J.; Howe, D. A study of soil erosion rates using [239]Pu, in the wet-dry tropics of Northern Australia. *J. Environ. Radioact.* **2020**, *211*, 106085. [CrossRef] [PubMed]

24. Velasco, H.; Astorga, R.T.; Joseph, D.; Antoine, J.S.; Mabit, L.; Toloza, A.; Dercon, G.; Walling, D.E. Adapting the Caesium-137 technique to document soil redistribution rates associated with traditional cultivation practices in Haiti. *J. Environ. Radioact.* **2018**, *183*, 7–16. [CrossRef]

25. Schoonejans, J.; Vanacker, V.; Opfergelt, S.; Christl, M. Long-term soil erosion derived from in-situ [10]Be and inventories of meteoric [10]Be in deeply weathered soils in southern Brazil. *Chem. Geol.* **2017**, *466*, 380–388. [CrossRef]

26. Wilken, F.; Fiener, P.; Ketterer, M.; Meusburger, K.; Muhindo, D.I.; van Oost, K.; Doetterl, S. Assessing soil redistribution of forest and cropland sites in wet tropical Africa using [239+240]Pu fallout radionuclides. *Soil* **2021**, *7*, 399–414. [CrossRef]

27. Waroszewski, J.; Egli, M.; Brandová, D.; Christl, M.; Kabala, C.; Malkiewicz, M.; Kierczak, J.; Glina, B.; Jezierski, P. Identifying slope processes over time and their imprint in soils of medium-high mountains of Central Europe (the Karkonosze Mountains, Poland). *Earth Surf. Process. Landf.* **2018**, *43*, 1195–1212. [CrossRef]

28. Mabit, L.; Bernard, C.; Laverdière, M.R. Assessment of erosion in the Boyer River watershed (Canada) using a GIS oriented sampling strategy and ^{137}Cs measurements. *Catena* **2007**, *71*, 242–249. [CrossRef]

29. Mabit, L.; Chhem-Kieth, S.; Toloza, A.; Vanwalleghem, T.; Bernard, C.; Amate, J.I.; González de Molina, M.; Gómez, J.A. Radioisotopic and physicochemical background indicators to assess soil degradation affecting olive orchards in southern Spain. *Agric. Ecosyst. Environ.* **2012**, *159*, 70–80. [CrossRef]

30. Meliho, M.; Nouira, A.; Benmansour, M.; Boulmane, M.; Khattabi, A.; Mhammdi, N.; Benkdad, A. Assessment of soil erosion rates in a Mediterranean cultivated and uncultivated soils using fallout [137]Cs. *J. Environ. Radioact.* **2019**, *208–209*, 106021. [CrossRef]

31. Quijano, L.; Beguería, S.; Gaspar, L.; Navas, A. Estimating erosion rates using ^{137}Cs measurements and WATEM/SEDEM in a Mediterranean cultivated field. *Catena* **2016**, *138*, 38–51. [CrossRef]

32. Jelinski, N.A.; Campforts, B.; Willenbring, J.K.; Schumacher, T.E.; Li, S.; Lobb, D.A.; Papiernik, S.K.; Yoo, K. Meteoric Beryllium-10 as a Tracer of Erosion Due to Postsettlement Land Use in West-Central Minnesota, USA. *J. Geophys. Res. Earth Surf.* **2019**, *124*, 874–901. [CrossRef]

33. Calitri, F.; Sommer, M.; Norton, K.; Temme, A.; Brandová, D.; Portes, R.; Christl, M.; Ketterer, M.E.; Egli, M. Tracing the temporal evolution of soil redistribution rates in an agricultural landscape using [239+240]Pu and [10]Be. *Earth Surf. Process. Landf.* **2019**, *44*, 1783–1789. [CrossRef]

34. Calitri, F.; Sommer, M.; van der Meij, M.W.; Egli, M. Soil erosion along a transect in a forested catchment: Recent or ancient processes? *Catena* **2020**, *194*, 104683. [CrossRef]

35. Ouimet, W.; Dethier, D.; Bierman, P.; Wyshnytzky, C.; Shea, N.; Rood, D.H. Spatial and temporal variations in meteoric [10]Be inventories and long-term deposition rates, Colorado Front Range. *Quat. Sci. Rev.* **2015**, *109*, 1–12. [CrossRef]

36. Tuo, D.; Xu, M.; Gao, G. Relative contributions of wind and water erosion to total soil loss and its effect on soil properties in sloping croplands of the Chinese Loess Plateau. *Sci. Total Environ.* **2018**, *633*, 1032–1040. [CrossRef]

37. Jagercikova, M.; Cornu, S.; Bourlès, D.; Antoine, P.; Mayor, M.; Guillou, V. Understanding long-term soil processes using meteoric [10]Be: A first attempt on loessic deposits. *Quat. Geochronol.* **2015**, *27*, 11–21. [CrossRef]

38. Poręba, G.J.; Śnieszko, Z.; Moska, P. Application of OSL dating and ^{137}Cs measurements to reconstruct the history of water erosion: A case study of a Holocene colluvium in Świerklany, south Poland. *Quat. Int.* **2015**, *374*, 189–197. [CrossRef]

39. Zhang, X.; Quine, T.A.; Walling, D.E. Soil erosion rates on sloping cultivated land on the Loess Plateau near Ansai, Shaanxi Province, China: An investigation using ^{137}Cs and rill measurements. *Hydrol. Process.* **1998**, *12*, 171–189. [CrossRef]

40. Loba, A.; Waroszewski, J.; Tikhomirov, D.; Calitri, F.; Christl, M.; Sykuła, M.; Egli, M. Tracing erosion rates in loess landscape of the Trzebnica Hills (Poland) over time using fallout and cosmogenic nuclides. *J. Soils Sediments* **2021**, *21*, 2952–2968. [CrossRef]

41. Kaste, J.M.; Elmore, A.J.; Vest, K.R.; Okin, G.S. Groundwater controls on episodic soil erosion and dust emissions in a desert ecosystem. *Geology* **2016**, *44*, 771–774. [CrossRef]

42. Abrahams, E.R.; Kaste, J.M.; Ouimet, W.; Dethier, D.P. Asymmetric hillslope erosion following wildfire in Fourmile Canyon, Colorado. *Earth Surf. Process. Landf.* **2018**, *43*, 2009–2021. [CrossRef]

43. McKean, J.A.; Dietrich, W.E.; Finkel, R.C.; Southon, J.R.; Caffee, M.W. Quantification of soil production and downslope creep rates from cosmogenic [10]Be accumulations on a hillslope profile. *Geology* **1993**, *21*, 343–346. [CrossRef]

44. Small, E.E.; Anderson, R.S.; Hancock, G.S. Estimates of the rate of regolith production using [10]Be and [26]Al from an alpine hillslope. *Geomorphology* **1999**, *27*, 131–150. [CrossRef]

45. Jungers, M.C.; Bierman, P.R.; Matmon, A.; Nichols, K.; Larsen, J.; Finkel, R. Tracing hillslope sediment production and transport with in situ and meteoric [10]Be. *J. Geophys. Res. Earth Surf.* **2009**, *114*, 1–16. [CrossRef]

46. West, N.; Kirby, E.; Bierman, P.; Slingerland, R.; Ma, L.; Rood, D.; Brantley, S. Regolith production and transport at the Susquehanna Shale Hills Critical Zone Observatory, Part 2: Insights from meteoric [10]Be. *J. Geophys. Res. Earth Surf.* **2013**, *118*, 1877–1896. [CrossRef]

47. West, N.; Kirby, E.; Bierman, P.; Clarke, B.A. Aspect-dependent variations in regolith creep revealed by meteoric [10]Be. *Geology* **2014**, *42*, 507–510. [CrossRef]

48. Graly, J.A.; Bierman, P.R.; Reusser, L.J.; Pavich, M.J. Meteoric [10]Be in soil profiles—A global meta-analysis. *Geochim. Cosmochim. Acta* **2010**, *74*, 6814–6829. [CrossRef]

49. Alewell, C.; Pitois, A.; Meusburger, K.; Ketterer, M.; Mabit, L. [239+240]Pu from "contaminant" to soil erosion tracer: Where do we stand? *Earth-Sci. Rev.* **2017**, *172*, 107–123. [CrossRef]

50. McHargue, L.R.; Damon, P.E. The global beryllium 10 cycle. *Rev. Geophys.* **1991**, *29*, 141. [CrossRef]

51. Monaghan, M.C.; Krishnaswami, S.; Turekian, K.K. The global-average production rate of [10]Be. *Earth Planet. Sci. Lett.* **1986**, *76*, 279–287. [CrossRef]

52. Willenbring, J.K.; von Blanckenburg, F. Meteoric cosmogenic Beryllium-10 adsorbed to river sediment and soil: Applications for Earth-surface dynamics. *Earth-Sci. Rev.* **2010**, *98*, 105–122. [CrossRef]

53. Beer, J.; McCracken, K.; von Steiger, R. *Cosmogenic Radionuclides. Theory and Applications in the Terrestial and Space Environments*; Physics of Earth and Space Environments; Springer: Berlin/Heidelberg, Germany, 2012; Volume 53, ISBN 978-3-642-14650-3.

54. Kaste, J.M.; Baskaran, M. Meteoric [7]Be and [10]Be as Process Tracers in the Environment. In *Handbook of Environmental Isotope Geochemistry*; Baskaran, M., Ed.; Advances in Isotope Geochemistry; Springer: Berlin/Heidelberg, Germany, 2012; Volume 1, pp. 61–85, ISBN 978-3-642-10636-1.

55. Graly, J.A.; Reusser, L.J.; Bierman, P.R. Short and long-term delivery rates of meteoric [10]Be to terrestrial soils. *Earth Planet. Sci. Lett.* **2011**, *302*, 329–336. [CrossRef]

56. Kaste, J.M.; Norton, S.A.; Hess, C.T. Environmental Chemistry of Beryllium-7. *Rev. Mineral. Geochem.* **2002**, *50*, 271–289. [CrossRef]

57. Pavich, M.J.; Brown, L.; Valette-Silver, J.N.; Klein, J.; Middleton, R. [10]Be analysis of a Quaternary weathering profile in the Virginia Piedmont. *Geology* **1985**, *13*, 39. [CrossRef]

58. Boschi, V.; Willenbring, J.K. Chemical and physical drivers of beryllium retention in two soil endmembers. *Sci. Total Environ.* **2021**, *754*, 141591. [CrossRef] [PubMed]

59. You, C.-F.; Lee, T.; Li, Y.-H. The partition of Be between soil and water. *Chem. Geol.* **1989**, *77*, 105–118. [CrossRef]

60. Pavich, M.J.; Brown, L.; Harden, J.; Klein, J.; Middleton, R. [10]Be distribution in soils from Merced River terraces, California. *Geochim. Cosmochim. Acta* **1986**, *50*, 1727–1735. [CrossRef]

61. Vesely, J.; Norton, S.A.; Skrivan, P.; Majer, V.; Kram, P.; Navratil, T.; Kaste, J.M. Environmental Chemistry of Beryllium. *Rev. Mineral. Geochem.* **2002**, *50*, 291–317. [CrossRef]

62. Bacon, A.R.; Richter, D.D.B.; Bierman, P.R.; Rood, D.H. Coupling meteoric [10]Be with pedogenic losses of [9]Be to improve soil residence time estimates on an ancient North American interfluve. *Geology* **2012**, *40*, 847–850. [CrossRef]

63. Pavich, M.J.; Brown, L.; Klein, J.; Middleton, R. [10]Be accumulation in a soil chronosequence. *Earth Planet. Sci. Lett.* **1984**, *68*, 198–204. [CrossRef]

64. Takahashi, Y.; Minai, Y.; Ambe, S.; Makide, Y.; Ambe, F. Comparison of adsorption behavior of multiple inorganic ions on kaolinite and silica in the presence of humic acid using the multitracer technique. *Geochim. Cosmochim. Acta* **1999**, *63*, 815–836. [CrossRef]

65. Ritchie, J.C.; McHenry, J.R. Application of Radioactive Fallout Cesium-137 for Measuring Soil Erosion and Sediment Accumulation Rates and Patterns: A Review. *J. Environ. Qual.* **1990**, *19*, 215–233. [CrossRef]

66. Xu, Y.; Qiao, J.; Pan, S.; Hou, X.; Roos, P.; Cao, L. Plutonium as a tracer for soil erosion assessment in northeast China. *Sci. Total Environ.* **2015**, *511*, 176–185. [CrossRef]

67. Nelson, D.M.; Lovett, M.B. Oxidation state of plutonium in the Irish Sea. *Nature* **1978**, *276*, 599–601. [CrossRef]

68. Penrose, W.R.; Metta, D.N.; Hylko, J.M.; Rinckel, L.A. The reduction of plutonium(V) by aquatic sediments. *J. Environ. Radioact.* **1987**, *5*, 169–184. [CrossRef]

69. Choppin, G.R. Actinide speciation in aquatic systems. *Mar. Chem.* **2006**, *99*, 83–92. [CrossRef]

70. Eakins, J.D.; Morgan, A.; Baston, G.M.N.; Pratley, F.W.; Strange, L.P.; Burton, P.J. Measurements of α-emitting plutonium and americium in the intertidal sands of West Cumbria, UK. *J. Environ. Radioact.* **1990**, *11*, 37–54. [CrossRef]

71. Iurian, A.-R.; Phaneuf, M.O.; Mabit, L. Mobility and Bioavailability of Radionuclides in Soils. In *Radionuclides in the Environment. Influence of Chemical Speciation and Plant Uptake on Radionuclide Migration*; Springer: Cham, Switzerland, 2015; pp. 38–59.

72. Kim, C.S.; Lee, M.H.; Kim, C.K.; Kim, K.H. $^{90}$Sr, $^{137}$Cs, $^{239+240}$Pu and $^{238}$Pu concentrations in surface soils of Korea. *J. Environ. Radioact.* **1998**, *40*, 75–88. [CrossRef]

73. Chibowski, S.; Zygmunt, J. The influence of the sorptive properties of organic soils on the migration rate of $^{137}$Cs. *J. Environ. Radioact.* **2002**, *61*, 213–223. [CrossRef]

74. Giannakopoulou, F.; Haidouti, C.; Chronopoulou, A.; Gasparatos, D. Sorption behavior of cesium on various soils under different pH levels. *J. Hazard. Mater.* **2007**, *149*, 553–556. [CrossRef] [PubMed]

75. Livens, F.R.; Loveland, P.J. The influence of soil properties on the environmental mobility of caesium in Cumbria. *Soil Use Manag.* **1988**, *4*, 69–75. [CrossRef]

76. Kabata-Pendias, A.; Mukherjee, A.B. (Eds.) *Trace Elements of Group 1 (Previously Group Ia) BT—Trace Elements from Soil to Human*; Springer: Berlin/Heidelberg, Germany, 2007; pp. 87–104, ISBN 978-3-540-32714-1.

77. Tamura, T.; Jacobs, D.G. Structural implications in cesium sorption. *Health Phys.* **1960**, *2*, 391—398. [CrossRef] [PubMed]

78. Bertsch, P.M. Cesium-137 in floodplain sediments of the Lower Three Runs Creek on the DOE Savannah River Site. *J. Radioanal. Nucl. Chem.* **2005**, *264*, 481–488. [CrossRef]

79. García-Oliva, F.; Lugo, R.M.; Maass, J.M. Soil $^{137}$Cs activity in a tropical deciduous ecosystem under pasture conversion in Mexico. *J. Environ. Radioact.* **1995**, *26*, 37–49. [CrossRef]

80. Van Bergeijk, K.E.; Noordijk, H.; Lembrechts, J.; Frissel, M.J. Influence of pH, soil type and soil organic matter content on soil-to-plant transfer of radiocesium and -strontium as analyzed by a nonparametric method. *J. Environ. Radioact.* **1992**, *15*, 265–276. [CrossRef]

81. Matisoff, G.; Whiting, P.J. Measuring Soil Erosion Rates Using Natural ($^7$Be, $^{210}$Pb) and Anthropogenic ($^{137}$Cs, $^{239,240}$Pu) Radionuclides. In *Handbook of Environmental Isotope Geochemistry*; Springer: Berlin/Heidelberg, Germany, 2012; Volume 1–2, pp. 487–519, ISBN 9783642106378.

82. Sanchez, A.L.; Wright, S.M.; Smolders, E.; Naylor, C.; Stevens, P.A.; Kennedy, V.H.; Dodd, B.A.; Singleton, D.L.; Barnett, C.L. High Plant Uptake of Radiocesium from Organic Soils Due to Cs Mobility and Low Soil K Content. *Environ. Sci. Technol.* **1999**, *33*, 2752–2757. [CrossRef]

83. Sheppard, S.C. Robust Prediction of Kd from Soil Properties for Environmental Assessment. *Hum. Ecol. Risk Assess. Int. J.* **2011**, *17*, 263–279. [CrossRef]

84. Wissocq, A.; Beaucaire, C.; Latrille, C. Application of the multi-site ion exchanger model to the sorption of Sr and Cs on natural clayey sandstone. *Appl. Geochem.* **2018**, *93*, 167–177. [CrossRef]

85. Siroux, B.; Beaucaire, C.; Tabarant, M.; Benedetti, M.F.; Reiller, P.E.; Wissocq, A.; Beaucaire, C.; Latrille, C. Adsorption of strontium and caesium onto an Na-MX80 bentonite: Experiments and building of a coherent thermodynamic modelling. *Appl. Geochem.* **2018**, *93*, 167–175. [CrossRef]

86. Nishiizumi, K.; Imamura, M.; Caffee, M.W.; Southon, J.R.; Finkel, R.C.; McAninch, J. Absolute calibration of $^{10}$Be AMS standards. *Nucl. Instrum. Methods Phys. Res. Sect. B Beam Interact. Mater. At.* **2007**, *258*, 403–413. [CrossRef]

87. Harden, J.W.; Fries, T.L.; Pavich, M.J. Cycling of beryllium and carbon through hillslope soils in Iowa. *Biogeochemistry* **2002**, *60*, 317–336. [CrossRef]

88. Knudsen, M.F.; Egholm, D.L.; Jansen, J.D. Time-integrating cosmogenic nuclide inventories under the influence of variable erosion, exposure, and sediment mixing. *Quat. Geochronol.* **2019**, *51*, 110–119. [CrossRef]

89. Meusburger, K.; Mabit, L.; Ketterer, M.; Park, J.H.; Sandor, T.; Porto, P.; Alewell, C. A multi-radionuclide approach to evaluate the suitability of $^{239+240}$Pu as soil erosion tracer. *Sci. Total Environ.* **2016**, *566–567*, 1489–1499. [CrossRef]

90. Mabit, L.; Martin, P.; Jankong, P.; Toloza, A.; Padilla-Alvarez, R.; Zupanc, V. Establishment of control site baseline data for erosion studies using radionuclides: A case study in East Slovenia. *J. Environ. Radioact.* **2010**, *101*, 854–863. [CrossRef]

91. Lal, D. New Nuclear Methods for Studies of Soil Dynamics Utilizing Cosmic Ray Produced Radionuclides. In *Sustaining the Global Farm-10th International Soil Conservation Organization Meeting*; Stott, D.E., Mohtar, R.H., Steinhardt, G.C., Eds.; Purdue University: West Lafayette, IN, USA; USDA-ARS National Soil Erosion Research Laboratory: Washington, DC, USA, 2001; pp. 1044–1052.

92. Campforts, B.; Vanacker, V.; Vanderborght, J.; Baken, S.; Smolders, E.; Govers, G. Simulating the mobility of meteoric $^{10}$Be in the landscape through a coupled soil-hillslope model (Be2D). *Earth Planet. Sci. Lett.* **2016**, *439*, 143–157. [CrossRef]

93. Owens, P.N.; Walling, D.E. Spatial variability of caesium-137 inventories at reference sites: An example from two contrasting sites in England and Zimbabwe. *Appl. Radiat. Isot.* **1996**, *47*, 699–707. [CrossRef]

94. Sutherland, R.A. Examination of caesium-137 areal activities in control (uneroded) locations. *Soil Technol.* **1991**, *4*, 33–50. [CrossRef]

95. Poręba, G.; Śnieszko, Z.; Moska, P.; Mroczek, P.; Malik, I. Interpretation of soil erosion in a Polish loess area using OSL, ^{137}Cs, [210]Pbex, dendrochronology and micromorphology—Case study: Biedrzykowice site (s Poland). *Geochronometria* **2019**, *46*, 57–78. [CrossRef]

96. Sarmiento, J.L.; Gwinn, E. Strontium 90 fallout prediction. *J. Geophys. Res.* **1986**, *91*, 7631. [CrossRef]

97. Poreba, G.J. Caesium-137 as a soil erosion tracer: A review. *Geochronometria* **2006**, *25*, 37–46.

98. Walling, D.E.; Quine, T.A. Calibration of caesium-137 measurements to provide quantitative erosion rate data. *Land Degrad. Dev.* **1990**, *2*, 161–175. [CrossRef]

99. Kachanoski, R.G.; de Jong, E. Predicting the Temporal Relationship between Soil Cesium-137 and Erosion Rate. *J. Environ. Qual.* **1984**, *13*, 301–304. [CrossRef]

100. Zhang, X.; Higgit, D.L.; Walling, D.E. A preliminary assessment of the potential for using caesium-137 to estimate rates of soil erosion in the Loess Plateau of China. *Hydrol. Sci. J.* **1990**, *35*, 243–252. [CrossRef]

101. Walling, D.E.; He, Q. Improved Models for Estimating Soil Erosion Rates from Cesium-137 Measurements. *J. Environ. Qual.* **1999**, *28*, 611–622. [CrossRef]

102. He, Q.; Walling, D.E. The distribution of fallout ^{137}Cs and ^{210}Pb in undisturbed and cultivated soils. *Appl. Radiat. Isot.* **1997**, *48*, 677–690. [CrossRef]

103. Owens, P.N.; Walling, D.E. The use of a numerical mass-balance model to estimate rates of soil redistribution on uncultivated land from ^{137}Cs measurements. *J. Environ. Radioact.* **1998**, *40*, 185–203. [CrossRef]

104. Van Oost, K.; Govers, G.; Van Muysen, W. A process-based conversion model for caesium-137 derived erosion rates on agricultural land: An integrated spatial approach. *Earth Surf. Process. Landf.* **2003**, *28*, 187–207. [CrossRef]

105. Mietelski, J.W.; Was, B. Plutonium from Chernobyl in Poland. *Appl. Radiat. Isot.* **1995**, *46*, 1203–1211. [CrossRef]

106. Ketterer, M.E.; Zheng, J.; Yamada, M. Applications of Transuranics as Tracers and Chronometers in the Environment. In *Handbook of Environmental Isotope Geochemistry*; Springer: Berlin/Heidelberg, Germany, 2012; Volume 1–2, pp. 395–417, ISBN 9783642106378.

107. Zheng, J.; Tagami, K.; Watanabe, Y.; Uchida, S.; Aono, T.; Ishii, N.; Yoshida, S.; Kubota, Y.; Fuma, S.; Ihara, S. Isotopic evidence of plutonium release into the environment from the Fukushima DNPP accident. *Sci. Rep.* **2012**, *2*, 304. [CrossRef]

108. Kelley, J.M.; Bond, L.A.; Beasley, T.M. Global distribution of Pu isotopes and [237]Np. *Sci. Total Environ.* **1999**, *237–238*, 483–500. [CrossRef]

109. Ketterer, M.E.; Hafer, K.M.; Link, C.L.; Kolwaite, D.; Wilson, J.; Mietelski, J.W. Resolving global versus local/regional Pu sources in the environment using sector ICP-MS. *J. Anal. At. Spectrom.* **2004**, *19*, 241–245. [CrossRef]

110. Mabit, L.; Benmansour, M.; Walling, D.E. Comparative advantages and limitations of the fallout radionuclides ^{137}Cs, [210]Pbex and [7]Be for assessing soil erosion and sedimentation. *J. Environ. Radioact.* **2008**, *99*, 1799–1807. [CrossRef] [PubMed]

111. Mabit, L.; Dercon, G.; Benmansour, M.; Walling, D.E. Use of ^{137}Cs,[210]Pbex and [7]Be for documenting soil redistribution: The future. In *Guidelines for Using Fallout Radionuclides to Assess Erosion and Effectiveness of Soil Conservation Strategies*; IAEA-TECDOC-1741; IAEA: Vienna, Austria, 2014; pp. 203–208, ISBN 978–92–0–105414–2.

112. Pennock, D.J.; Lemmen, D.S.; De Jong, E. Cesium-137-measured erosion rates for soils of five parent-material groups in southwestern Saskatchewan. *Can. J. Soil Sci.* **1995**, *75*, 205–210. [CrossRef]

113. Monaghan, M.C.; Krishnaswami, S.; Thomas, J.H. [10]Be concentrations and the long-term fate of particle-reactive nuclides in five soil profiles from California. *Earth Planet. Sci. Lett.* **1983**, *65*, 51–60. [CrossRef]

114. Van Pelt, R.S.; Zobeck, T.M.; Ritchie, J.C.; Gill, T.E. Validating the use of ^{137}Cs measurements to estimate rates of soil redistribution by wind. *Catena* **2007**, *70*, 455–464. [CrossRef]

115. Schuller, P.; Walling, D.; Sepúlveda, A.; Trumper, R.; Rouanet, J.; Pino, I.; Castillo, A. Use of ^{137}Cs measurements to estimate changes in soil erosion rates associated with changes in soil management practices on cultivated land. *Appl. Radiat. Isot.* **2004**, *60*, 759–766. [CrossRef]

116. Evans, R.; Collins, A.L.; Zhang, Y.; Foster, I.D.L.; Boardman, J.; Sint, H.; Lee, M.R.F.; Griffith, B.A. A comparison of conventional and ^{137}Cs-based estimates of soil erosion rates on arable and grassland across lowland England and Wales. *Earth-Sci. Rev.* **2017**, *173*, 49–64. [CrossRef]

117. Quijano, L.; Gaspar, L.; Navas, A. Spatial patterns of SOC, SON, ^{137}Cs and soil properties as affected by redistribution processes in a Mediterranean cultivated field (Central Ebro Basin). *Soil Tillage Res.* **2016**, *155*, 318–328. [CrossRef]

118. Benmansour, M.; Mabit, L.; Nouira, A.; Moussadek, R.; Bouksirate, H.; Duchemin, M.; Benkdad, A. Assessment of soil erosion and deposition rates in a Moroccan agricultural field using fallout ^{137}Cs and [210]Pbex. *J. Environ. Radioact.* **2013**, *115*, 97–106. [CrossRef]

119. Porto, P.; Callegari, G. Using ^{137}Cs measurements to estimate soil erosion rates in forest stands affected by wildfires. Results from plot experiments. *Appl. Radiat. Isot.* **2021**, *172*, 109668. [CrossRef]

120. Saç, M.M.; İçhedef, M. Application of ^{137}Cs technique for evaluation of erosion and deposition rates within cultivated fields of Salihli region, Western Turkey. *J. Radiat. Res. Appl. Sci.* **2015**, *8*, 477–482. [CrossRef]

121. Zhang, W.; Xing, S.; Hou, X. Evaluation of soil erosion and ecological rehabilitation in Loess Plateau region in Northwest China using plutonium isotopes. *Soil Tillage Res.* **2019**, *191*, 162–170. [CrossRef]

122. Zhang, K.; Pan, S.; Liu, Z.; Li, G.; Xu, Y.; Hao, Y. Vertical distributions and source identification of the radionuclides [239]Pu and [240]Pu in the sediments of the Liao River estuary, China. *J. Environ. Radioact.* **2018**, *181*, 78–84. [CrossRef]

123. Li, M.; Li, Z.; Liu, P.; Yao, W. Using Cesium-137 technique to study the characteristics of different aspect of soil erosion in the Wind-water Erosion Crisscross Region on Loess Plateau of China. *Appl. Radiat. Isot.* **2005**, *62*, 109–113. [CrossRef] [PubMed]

124. Gharibreza, M.; Zaman, M.; Porto, P.; Fulajtar, E.; Parsaei, L.; Eisaei, H. Assessment of deforestation impact on soil erosion in loess formation using $^{137}$Cs method (case study: Golestan Province, Iran). *Int. Soil Water Conserv. Res.* **2020**, *8*, 393–405. [CrossRef]

125. Hua-juni, F.; Xue-ming, Y.; Xiao-ping, Z.; Ai-zhenl, L. Using $^{137}$Cs Tracer Technique to Evaluate Erosion and Deposition of Black Soil in Northeast China. *Pedosphere* **2006**, *16*, 201–209.

126. Yang, M.-Y.; Tian, J.-L.; Liu, P.-L. Investigating the spatial distribution of soil erosion and deposition in a small catchment on the Loess Plateau of China, using $^{137}$Cs. *Soil Tillage Res.* **2006**, *87*, 186–193. [CrossRef]

127. Fifield, L.K.; Wasson, R.J.; Pillans, B.; Stone, J.O.H. The longevity of hillslope soil in SE and NW Australia. *Catena* **2010**, *81*, 32–42. [CrossRef]

128. Hoo, W.T.; Fifield, L.K.; Tims, S.G.; Fujioka, T.; Mueller, N. Using fallout plutonium as a probe for erosion assessment. *J. Environ. Radioact.* **2011**, *102*, 937–942. [CrossRef]

129. Arata, L.; Alewell, C.; Frenkel, E.; A'Campo-Neuen, A.; Iurian, A.R.; Ketterer, M.E.; Mabit, L.; Meusburger, K. Modelling Deposition and Erosion rates with RadioNuclides (MODERN)—Part 2: A comparison of different models to convert $^{239+240}$Pu inventories into soil redistribution rates at unploughed sites. *J. Environ. Radioact.* **2016**, *162–163*, 97–106. [CrossRef] [PubMed]

130. Musso, A.; Ketterer, M.E.; Greinwald, K.; Geitner, C.; Egli, M. Rapid decrease of soil erosion rates with soil formation and vegetation development in periglacial areas. *Earth Surf. Process. Landforms* **2020**, *45*, 2824–2839. [CrossRef]

131. Schmidt, S.; Alewell, C.; Meusburger, K. Monthly RUSLE soil erosion risk of Swiss grasslands. *J. Maps* **2019**, *15*, 247–256. [CrossRef]

132. Lu, H.; Prosser, I.P.; Moran, C.J.; Gallant, J.C.; Priestley, G.; Stevenson, J.G. Predicting sheetwash and rill erosion over the Australian continent. *Soil Res.* **2003**, *41*, 1037. [CrossRef]

133. Panagos, P.; Borrelli, P.; Poesen, J.; Ballabio, C.; Lugato, E.; Meusburger, K.; Montanarella, L.; Alewell, C. The new assessment of soil loss by water erosion in Europe. *Environ. Sci. Policy* **2015**, *54*, 438–447. [CrossRef]

134. Fu, B.; Liu, Y.; Lü, Y.; He, C.; Zeng, Y.; Wu, B. Assessing the soil erosion control service of ecosystems change in the Loess Plateau of China. *Ecol. Complex.* **2011**, *8*, 284–293. [CrossRef]

135. Yang, X.M.; Zhang, X.P.; Deng, W.; Fang, H.J. Black soil degradation by rainfall erosion in Jilin, China. *Land Degrad. Dev.* **2003**, *14*, 409–420. [CrossRef]

136. Borrelli, P.; Robinson, D.A.; Fleischer, L.R.; Lugato, E.; Ballabio, C.; Alewell, C.; Meusburger, K.; Modugno, S.; Schütt, B.; Ferro, V.; et al. An assessment of the global impact of 21st century land use change on soil erosion. *Nat. Commun.* **2017**, *8*, 2013. [CrossRef]

137. Sun, W.; Shao, Q.; Liu, J.; Zhai, J. Assessing the effects of land use and topography on soil erosion on the Loess Plateau in China. *Catena* **2014**, *121*, 151–163. [CrossRef]

138. Ayt Ougougdal, H.; Khebiza, M.Y.; Messouli, M.; Bounoua, L.; Karmaoui, A. Delineation of vulnerable areas to water erosion in a mountain region using SDR-InVEST model: A case study of the Ourika watershed, Morocco. *Sci. Afr.* **2020**, *10*, e00646. [CrossRef]

139. Sheikh, V.; Kornejady, A.; Ownegh, M. Application of the coupled TOPSIS–Mahalanobis distance for multi-hazard-based management of the target districts of the Golestan Province, Iran. *Nat. Hazards* **2019**, *96*, 1335–1365. [CrossRef]

140. Fülöp, R.H.; Bishop, P.; Fabel, D.; Cook, G.T.; Everest, J.; Schnabel, C.; Codilean, A.T.; Xu, S. Quantifying soil loss with in-situ cosmogenic$^{10}$Be and $^{14}$C depth-profiles. *Quat. Geochronol.* **2015**, *27*, 78–93. [CrossRef]

141. Arnhold, S.; Lindner, S.; Lee, B.; Martin, E.; Kettering, J.; Nguyen, T.T.; Koellner, T.; Ok, Y.S.; Huwe, B. Conventional and organic farming: Soil erosion and conservation potential for row crop cultivation. *Geoderma* **2014**, *219–220*, 89–105. [CrossRef]

142. Meusburger, K.; Konz, N.; Schaub, M.; Alewell, C. Soil erosion modelled with USLE and PESERA using QuickBird derived vegetation parameters in an alpine catchment. *Int. J. Appl. Earth Obs. Geoinf.* **2010**, *12*, 208–215. [CrossRef]

143. Meusburger, K.; Evrard, O.; Alewell, C.; Borrelli, P.; Cinelli, G.; Ketterer, M.; Mabit, L.; Panagos, P.; van Oost, K.; Ballabio, C. Plutonium aided reconstruction of caesium atmospheric fallout in European topsoils. *Sci. Rep.* **2020**, *10*, 11858. [CrossRef]

144. Arata, L.; Meusburger, K.; Frenkel, E.; A'Campo-Neuen, A.; Iurian, A.R.; Ketterer, M.E.; Mabit, L.; Alewell, C. Modelling Deposition and Erosion rates with RadioNuclides (MODERN)—Part 1: A new conversion model to derive soil redistribution rates from inventories of fallout radionuclides. *J. Environ. Radioact.* **2016**, *162–163*, 45–55. [CrossRef]

145. Schaub, M.; Konz, N.; Meusburger, K.; Alewell, C. Application of in-situ measurement to determine $^{137}$Cs in the Swiss Alps. *J. Environ. Radioact.* **2010**, *101*, 369–376. [CrossRef]

146. Evrard, O.; Vandaele, K.; van Wesemael, B.; Bielders, C.L. A grassed waterway and earthen dams to control muddy floods from a cultivated catchment of the Belgian loess belt. *Geomorphology* **2008**, *100*, 419–428. [CrossRef]

147. Haase, D.; Fink, J.; Haase, G.; Ruske, R.; Pécsi, M.; Richter, H.; Altermann, M.; Jäger, K.D. Loess in Europe-its spatial distribution based on a European Loess Map, scale 1:2,500,000. *Quat. Sci. Rev.* **2007**, *26*, 1301–1312. [CrossRef]

148. Šimanský, V.; Juriga, M.; Mendyk, Ł. Slope position and management practices as factors influencing selected properties of topsoil. *Soil Sci. Annu.* **2019**, *70*, 137–146. [CrossRef]

149. Licznar, M.; Kowaliński, S.; Drozd, J. Changes of some physical properties of soils of the głubczyce plateau under the water erosion effect. *Rocz. Glebozn.* **1981**, *XXXII*, 45–52.

150. Poręba, G.; Śnieszko, Z.; Moska, P. Some aspects of age assessment of Holocene loess colluvium: OSL and $^{137}$Cs dating of sediment from Biała agricultural area, South Poland. *Quat. Int.* **2011**, *240*, 44–51. [CrossRef]

151. Zhang, J.; Yang, M.; Sun, X.; Zhang, F. Estimation of wind and water erosion based on slope aspects in the crisscross region of the Chinese Loess Plateau. *J. Soils Sediments* **2018**, *18*, 1620–1631. [CrossRef]

152. Aldahan, A.; Haiping, Y.; Possnert, G. Distribution of beryllium between solution and minerals (biotite and albite) under atmospheric conditions and variable pH. *Chem. Geol.* **1999**, *156*, 209–229. [CrossRef]